Methods of measuring the moisture diffusivity at high moisture levels

Janz, Mårten

1997

UNIVERSITY OF LUND
LUND INSTITUTE OF TECHNOLOGY
Division of Building Materials

METHODS OF MEASURING THE MOISTURE DIFFUSIVITY AT HIGH MOISTURE LEVELS

MÅRTEN JANZ

Report TVBM-3076 Licentiate Thesis
Lund 1997

ISRN: LUTVDG/TVBM--97/3076—SE(1-73)
ISSN: 0348-7911 TVBM

Lund Institute of Technology
Division of Building Materials
Box 118
S-221 00 Lund, Sweden

Telephone: +46-46-2227415
Telefax: +46-46-2224427
WWW: http://www.ldc.lu.se/lthbml

Preface

This work has been carried out at the Division of Building Materials at the Lund Institute of Technology and has been financed by the Swedish Council for Building Research. The research project was a part of the Moisture Research Group in Lund and was initiated by my supervisor Professor Göran Fagerlund, whom I wish to thank for his support.

I also wish to express my gratitude to Dr Johan Claesson who came up with the original idea for the type of tests performed in this study. I would also like to thank all the staff at the Division of Building Materials for their help and support during the process.

Contents

Summary

The purpose of this licentiate study is to analyze capillarity transport in building materials, and in order to do that, develop a new measurement method by which the moisture diffusivity at high moisture levels can be measured in an easy way.

The material used in this development procedure was a sedimentary calcareous sandstone named Uddvide emanating from the island of Gotland. The porosity and density of the sandstone were measured to 23% and 2059 kg/m^3, respectively.

Two new evaluation methods to determine the moisture diffusivity at high moisture contents have been developed. From the first method the moisture diffusivities are calculated exactly. This method is based on the Boltzmann-transformation and was first presented by Claesson (1994). The second method is based on an analytical solution of step response with two moisture capacities given in (Arfvidsson 1994). This method gives an approximate solution of the Kirchhoff flow potential. The advantage of this method is that the calculations are easy and quick to perform. A presumption for both methods is that the moisture flow can be mathematically described by Fick's law, i.e. the moisture flow is linearly proportional to the gradient of the water content.

Both methods give reasonable and rather similar results at high water contents, but it seems as if neither of the methods is useful on the actual sandstone at low moisture contents. Both methods must therefore be supplemented by the measurement of the moisture diffusivity at low moisture levels, e.g. by measurements performed by the cup-method. However, the purpose of this work was to find a measurement method to determine the moisture diffusivity at high moisture contents which cannot be obtained by traditional methods.

The input used in both methods described is a series of sorption coefficients, A_1, A_2,..., A_N [kg/(m^2·s^{½})], corresponding to different initial water contents, $w_{in} = w_1, w_2,..., w_N$ [kg/m^3] and to the water content at capillary saturation, w_{cap}. Thus, the only experiment that must be carried out is a series of capillary water uptake tests performed on pre-conditioned specimens with no initial moisture gradients. This entails a limited technical effort, principally the only equipment needed is a balance. The laboratory set-up used in this study recorded automatically, on-line, the amount of absorbed water.

If the two methods of evaluating the moisture diffusivity from the relation $A(w_{in})$ are to be of an extensive use, a rapid method of conditioning the specimens must be used. A method for this was developed. The specimens were conditioned by letting them suck water to the desired initial moisture content whereupon they were sealed and stored in at least 14 days before the capillary water uptake test was performed. To what extent this rapid conditioning method results in moisture gradients that influence the capillary water test was however uncertain. Therefore, the results of capillary water uptake tests performed on specimens conditioned with this rapid method were compared with two other conditioning methods; one in the hygroscopic range and one in the superhygroscopic range. Moisture gradients in the specimen body were prevented with these two conditioning methods since the specimens were conditioned through absorption or desorption from considerably lower and higher moisture contents than the initial moisture content aimed at. Conditioning was made by letting the material reach equilibrium with a certain pore water pressure.

In the hygroscopic range the specimens were conditioned both by absorption and desorption in eight different climate chambers. Different saturated salt solutions were used to obtain the desired relative humidity in the climate chambers. In the superhygroscopic range the specimens were conditioned in an ”extractor”. The water was forced out of the capillary saturated specimen by an applied air pressure. The conditioning also resulted in information about the sorption isotherm (moisture content versus relative humidity, RH) and the water retention curve (moisture content versus capillary pressure) of the sandstone. These two measurements of the moisture storage capacity were related to each other by the Kelvin equation.

No significant difference were noticed between the different methods of conditioning. This indicates that there was not any moisture gradient in the specimen body after the rapid conditioning, thus, this seems to be suitable on the sandstone used in this study.

Nomenclature

All symbols are explained where they first appear in the text. Most of the symbols are also presented here. As far as is possible the symbols recommended by ISO 9346: 1987 (E) have been used. All dimensions are in SI units.

Symbol	Definition	Dimension
A	Sorption coefficient	$kg/(m^2 \cdot s^{½})$
B	Water penetration coefficient	$m/s^{½}$
C	Moisture capacity	s/m^2
$D_{cup,\ max}$	Moisture diffusivity obtained with the cup-method at $w_{cup,max}$	m^2/s
D_w	Moisture diffusivity with w used as potential	m^2/s
g	Density of moisture flow rate	$kg/(m^2 \cdot s)$
k_p	Permeability	kg/m
ℓ	Specimen length	m
M	Water penetration resistance	s/m^2
M_w	Molar weight of water (0.018 kg/mol)	kg/mol
m_{air}	Weight in air of a vacuum saturated specimen	kg
m_{in}	Initial mass	kg
m_w	Weight in water of a vacuum saturated specimen	kg
m_0	Dry mass	kg
P	Pressure	Pa
P_{air}	Applied air pressure	Pa
P_{atm}	Atmospheric pressure	Pa
P_{cap}	Capillary pressure	Pa
P_ℓ	Pore water pressure	Pa
p_s	Saturation vapour pressure	Pa
p_v	Vapour pressure	Pa
R	Gas constant (8.314 J/(mol·K))	J/(mol·K)
r	Radius of a meniscus	m
r_0	Pore radius	m
T	Temperature	K
S	Surface area	m^2
t	Time	s
t_c	Time until the specimen becomes capillary saturated	s
u	Moisture content mass by mass	kg/kg
u_{in}	Initial water content mass by mass	kg/kg
V	Volume	m^3
v	Vapour content	kg/m^3
W	Amount of absorbed water per square meter	kg/m^2
w	Moisture content mass by volume	kg/m^3

w_{cap}	Moisture content at capillary saturation mass by volume	kg/m^3
$w_{cup,\ max}$	The highest moisture content used with the cup-method	kg/m^3
w_{in}	Initial moisture content mass by volume	kg/m^3
w_{ref}	Moisture content at a reference level	kg/m^3
δ_p	Moisture permeability with p_v used as potential	kg/(m·s·Pa)
δ_v	Moisture permeability with v used as potential	m^2/s
ε	Moisture content volume by volume	m^3/m^3
Φ	Porosity	m^3/m^3
Φ_a	Active porosity available for capillary transport	m^3/m^3
Φ_c	Capillary porosity	m^3/m^3
η	Dynamic viscosity	Pa·s
φ	Relative humidity	-
θ	Contact angle	rad
ρ	Density	kg/m^3
ρ_c	Compact density	kg/m^3
ρ_w	Density of water	kg/m^3
σ	Surface tension	N/m
Ψ	Soil water potential	J/kg or m
ψ	Kirchhoffs flow potential	kg/(m·s)
ψ_{cap}	Kirchhoffs flow potential at capillary saturation	kg/(m·s)
$\psi_{cup,\ max}$	Kirchhoffs flow potential obtained with the cup-method at $w_{cup,\ max}$	kg/(m·s)
ψ_{ref}	Kirchhoffs flow potential at a reference level	kg/(m·s)

1 Introduction

Moisture in porous building materials plays an important role in almost all durability problems. In many cases, moisture is the direct cause of damage. Moisture is also important in a variety of other degradation processes where it serves as a catalyst (e.g. in connection with emission of unhealthy substances from flooring materials). Society incurs considerable costs yearly, because of durability problems.

Several of the durability problems are strongly connected with very high moisture contents in the material. Such moisture contents can only be obtained by capillary suction, or occur at very high relative humidity. Examples are frost attack, steel corrosion, rot of timber, and mold. For an accurate service life prediction, it is therefore very important to have good models for the moisture transport. It is also important to know the corresponding transport properties at these high moisture levels.

Chapter 2 presents different mathematical models proposed in the literature, that describe the moisture transport. Both isothermal and non-isothermal modes are discussed. In the hygroscopic range several well documented measurement methods for moisture diffusivity are available (see Hedenblad, 1993). At high moisture levels there are no such well documented measurement methods. Principally, however, the moisture diffusivity can be calculated from transient moisture distributions, and there exist different measurement techniques to measure these distributions. Some of them are briefly described in Chapter 3. In that chapter a method is presented to evaluate the moisture diffusivity from steady state moisture profiles. An approximate method is also presented there, to evaluate the moisture diffusivity from the sorption coefficient.

There are disadvantages with all existing measurement techniques described in Chapter 3; (i) a major technical effort is required to measure transient moisture profiles, (ii) steady state measurements are very time demanding, (iii) the approximate methods available are not accurate enough for many applications. The need is obvious, for an easy test method by which the moisture diffusivity at high moisture levels can be measured.

Two new techniques to evaluate the moisture diffusivity at high moisture levels have therefore been developed. One method is exact, and the other is approximate. The experimental set-up is simple. Principally, the only equipment needed is a balance. That is because the moisture diffusivity and the Kirchhoff flow potential are calculated from a series of sorption coefficients. These coefficients are obtained by weighing the specimen in a number of capillary absorption tests. The experimental set-up is described in Chapter 4. Both theories used to evaluate the moisture diffusivity are described in Chapter 5. The exact method, based on the Boltzmann-transformation, was first presented by Claesson, (1994). The approximate method is based on an analytical solution of step response with two capacities. The method is given in Arfvidsson (1994). The evaluation is performed using both described methods. The results are compared in Chapter 5.

2 Theory

2.1 Basic capillary theory

Surface tension between water and air is caused by the attraction forces acting on the molecules of the liquid. The magnitude of the attraction decreases strongly with increasing distance between the molecules. This distance is considerable larger in a gas than in a liquid. Therefore, liquid molecules at the surface are more attracted towards the interior liquid than towards a surrounding gas. Contrary to the forces acting on molecules at the surface, the forces among the liquid molecules within the bulk are balanced by one another. The liquid will therefore tend to form a relatively tough ”skin” or film on its surface and minimize the surface area by striving to form a spherical drop (a spherical shape contains the maximum number of molecules within the bulk volume**)**. Energy is needed to transport a molecule from the bulk to the surface. This energy per unit area is numerically the *surface tension* σ. The units of surface tension are J/m^2 or N/m (J = Nm). The surface tension between water and air at different temperatures is shown in Table 2.1. Surface tension will also occur in a similar way at the solid material/liquid interface, and at the solid material/gas interface.

Between the edge of the meniscus and the solid material is a *contact angle* θ (see Figure 2.1 and Figure 2.2). This contact angle results from the balance among the three surface tensions acting at the interface between liquid, solid and gas **(**see Figure 2.2**).** Thus, the contact angle is a function of the characteristics of both the liquid, gas and the solid material. The forces in Figure 2.2 are balanced if

$$\sigma_{sg} = \sigma_{sl} + \sigma_{lg}\cos\theta \tag{2.1}$$

where the indices *sg*, *sl* and *lg* denote the solid/gas, solid/liquid and liquid/gas interfaces, respectively. The contact angle can be solved, obtaining

$$\cos\theta = \frac{\sigma_{sg} - \sigma_{sl}}{\sigma_{lg}} \tag{2.2}$$

If $0 < \theta < 90°$ the surface is *hydrophile* and $\sigma_{sl} < \sigma_{sg}$. If $\theta = 0$ the liquid wets the solid surface fully and $\sigma_{sg} = \sigma_{lg}$ which in turn means that no work (energy) is needed to create the solid/liquid interface. If $\theta > 90°$ the surface is *hydrophobic*. In the special case when $\theta = 180°$, no work is needed to create the solid/gas interface. In this case, σ_{sg} will be equal to zero. This means that a drop of liquid on the surface of the solid remains separated by a thin film of vapor (Atkins 1994).

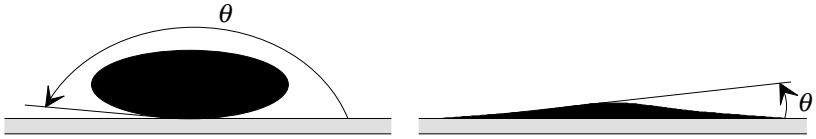

Figure 2.1 A liquid drop on a hydrophobic (left) and on a hydrophile surface (right).

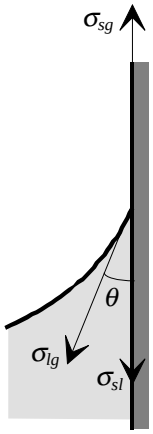

Figure 2.2 The balance of forces that results in a contact angle θ.

In a small tube connected to a liquid reservoir, a meniscus will be formed. A pressure difference over the meniscus will appear. If the surface of the tube is hydrophile, there will be an under-pressure in the liquid and the liquid will penetrate the tube. The magnitude of the pressure difference over a meniscus can be calculated from the driving force F [N] acting on the water. The driving force, in turn, is calculated as the product of the circumference of the tube and the vertical component of the liquid/gas surface tension. In this way, the driving force for a circular tube is given by:

$$F = 2\pi r_0 \sigma \cos\theta \tag{2.3}$$

where

- σ is the surface tension between liquid and gas (the index *lg* will henceforth not be used) [N/m];
- θ is the contact angle;
- r_0 is the tube radius [m].

By dividing the driving force F [N] by the sectional area of the circular tube, the under-pressure, or capillary pressure P_{cap} [Pa] is determined:

$$P_{cap} = \frac{2\sigma \cos\theta}{r_0} \tag{2.4}$$

In a pore with a cross section that is not circular, a more general expression for the capillary pressure can be designated. Equilibrium of forces requires that:

$$P_{cap} = \sigma \cos\theta \cdot \left(\frac{1}{r_1} + \frac{1}{r_2} \right) \tag{2.5}$$

where r_1 and r_2 are the principal radii of the meniscus in two orthogonal directions. Eq. 2.5 is known as the Laplace formula for capillary pressure.

At equilibrium in a vertical tube, the underpressure below the meniscus is balanced by the pressure caused by the weight of the water column:

$$\rho g_{acc} h = \frac{2\sigma \cos\theta}{r_0} \tag{2.6}$$

where g_{acc} is the acceleration due to gravity [m/s^2]. The height h [m] at equilibrium then is:

$$h = \frac{2\sigma \cos\theta}{r_0 \rho g_{acc}} \tag{2.7}$$

Thus, the height at equilibrium is (among other things) a function of the pore radius. Figure 2.3 shows the height of water at equilibrium in a circular tube with a zero contact angle, as a function of the tube radius (most of the building materials are hydrophile and the contact angle is often approximated as zero). In a pore with varying radius, the height at equilibrium can be different depending on whether water in the pore is absorbed from a dry state or desorbed from a saturated state (see Figure 2.4).

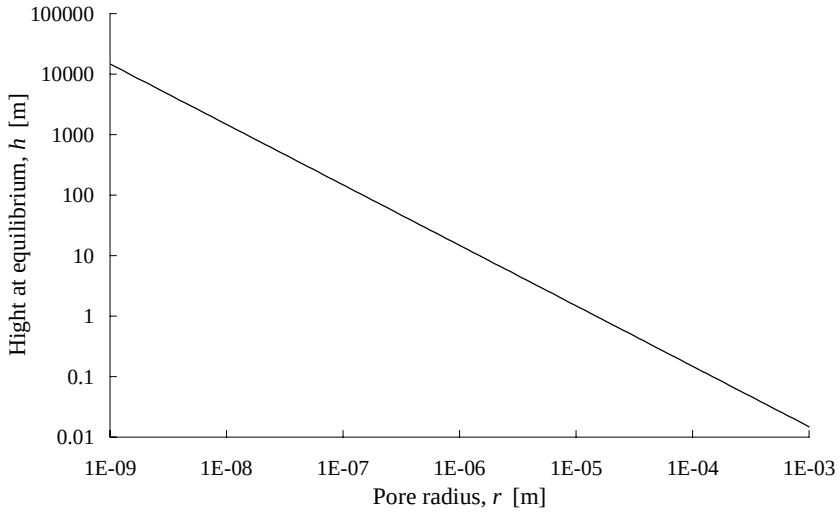

Figure 2.3 The height at equilibrium for water in a circular tube as a function of the tube radius (θ = 0).

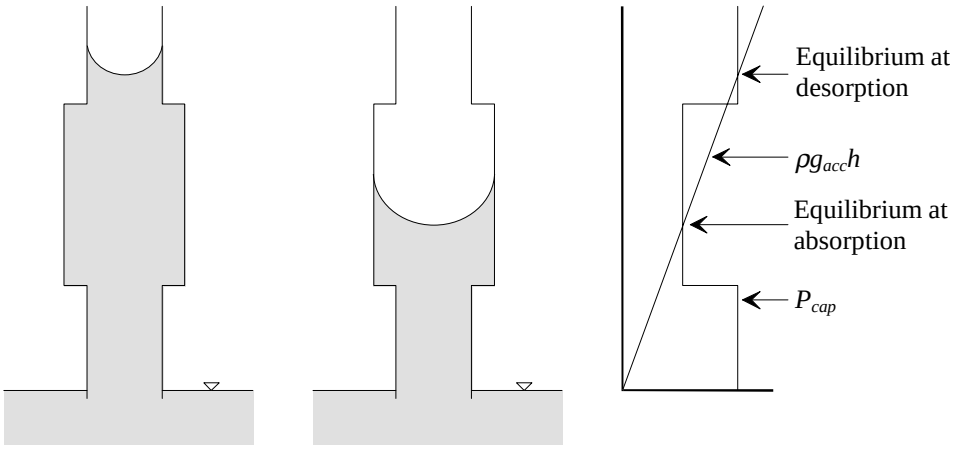

Figure 2.4 Equilibrium height in a pore undergoing desorption (left) and absorption (right).

The laminar flow g [kg/(m^2·s)] of a liquid with a viscosity η [Pa·s] in a cylindrical tube of radius r_0 [m] and length L [m] is given by the Poiseuille law:

$$g = -\frac{r_0^2 \rho}{8\eta} \frac{dP}{dx} \tag{2.8}$$

Poiseuille's law is a well known solution of the Navier-Stokes equation of laminar flow in a tube. From Poiseuille's law the movement of the meniscus can be derived. The driving pressure gradient in a horizontal tube is:

$$\frac{dP}{dx} = -\frac{P_{cap}}{x} \tag{2.9}$$

where

P_{cap} is the capillary pressure given by Eq. 2.4;
x is the penetration depth of the meniscus in the tube.

The velocity $v = \frac{g}{\rho} = \frac{dx}{dt}$ [m/s] of the meniscus becomes:

$$\frac{dx}{dt} = \frac{r_0 \sigma \cos\theta}{4\eta x} \tag{2.10}$$

Integration gives:

$$t = \frac{2\eta}{r_0 \sigma \cos\theta} \cdot x^2 \tag{2.11}$$

This is the time it will take for the meniscus to reach the depth x in a horizontal cylindrical tube.

This is basic capillary theory, used on a single tube. It is obviously of limited use for the capillary flow in a porous building material, with its very complex pore system. The basic theory shows, however, which material characteristics are involved. It also shows how these characteristics influence the capillary flow (i.e. the basic capillary theory is indispensable in order to understand capillarity transport in porous materials).

Table 2.1 Surface tension σ between water and air, viscosity of water η and density of water ρ_w (at 1 atm) at various temperatures (Weast et al. 1989).

Temperature [°C]	Surface tension, σ [N/m]	Viscosity, η [Pa·s]	Density of water, ρ_w [kg/m^3]
0	0.0756	0.001787	999.8395
5	0.0749	0.001519	999.9638
10	0.07422	0.001307	999.6996
15	0.07349	0.001139	999.0996
20	0.07275	0.001002	998.2041
23	-	0.0009325	997.5385
25	0.07197	0.0008904	997.0449
30	0.07118	0.0007975	995.6473
50	0.06791	0.0005468	988.0363
70	0.0644	0.0004042	977.7696
100	0.0589	0.0002818	958.3637

2.2 Moisture transport in porous materials

2.2.1 General

The transport phenomena in porous media can be separated into *diffusion*, *saturated viscous flow* and *capillary (liquid) transport*.

Diffusion at isothermal conditions is driven by a difference in vapour pressure, i.e. the water molecules are moving towards a lower vapour pressure. The most common way to describe the three-dimensional diffusion process is by Fick's law:

$$g = -\delta_p \nabla p_v \tag{2.12}$$

which in one dimension becomes:

$$g = -\delta_p \frac{\partial p_v}{\partial x} \tag{2.13}$$

where

g is the density of moisture flow rate [kg/(m^2·s)]
δ_p is the moisture permeability [kg/(m·s·Pa)];
p_v is the vapour pressure [Pa].

The moisture permeability is a function of the vapour pressure, i.e. $\delta_p = f(p_v)$.

Viscous saturated flow is driven by a difference in pressure. The flow depends both on the geometry of the porous material and on properties of the fluid itself. The saturated flow g [kg/(m^2·s)] is often described by Darcy's law, which expressed in the three dimensional pressure field becomes:

$$g = -\frac{k_p}{\eta}\nabla P \tag{2.14}$$

For a one-dimensional case, Darcy's law becomes:

$$g = -\frac{k_P}{\eta}\frac{dP}{dx} \tag{2.15}$$

where k_P is the permeability [kg/m^2].

For diffusion and saturated flow in a porous material, Fick's law and Darcy's law are widely used and, for many applications, accepted. For *capillary liquid transport* through a porous material there is no such used and accepted relation.

2.2.2 Capillary transport

The simplest model of *capillary transport* is to approximate the wetted region as a fully saturated rectangular wet front, a 'sharp wet front' or 'moving boundary'. For many applications this model is accurate enough. Eq. 2.11 can then be used (more or less) directly:

$$x = B_{tube}\sqrt{t} \tag{2.16}$$

where

$$B_{tube} = \sqrt{\frac{r_0\,\sigma\cos\theta}{2\eta}} \tag{2.17}$$

These two equations are only valid for capillary transport in tubes. In a porous material the coefficient B cannot be expressed in the simple way that Eq. 2.17 suggests. The form of Eq. 2.16 can, however, still be used:

$$x = B\cdot\sqrt{t} \tag{2.18}$$

where x [m] is the penetration depth of the suggested sharp wet front and B [m/s^{½}] is the penetration coefficient which is to be determined experimentally. The magnitude of B is dependent on the geometry of the liquid-vapour menisci, the surface tension, the contact angle and the viscosity of the liquid. Since the geometry of the liquid-vapour menisci in turn is dependent on the degree of saturation, the penetration coefficient B will also be a function of the state of saturation in the material.

Assuming that the moisture penetration is a moving boundary the total amount of absorbed liquid W [kg/m^2] can be denoted by:

$$W = A\sqrt{t} \tag{2.19}$$

where the sorption coefficient A [kg/(m^2·s^{½})] is:

$$A = \rho\Phi_a B \tag{2.20}$$

and where

ρ is the liquid density [kg/m^3];
Φ_a is the active porosity available for capillary transport [m^3/m^3].

The flow rate $g_{x=0}$ [kg/(m^2·s)] through the material boundary exposed to the liquid is the time derivative of *W*. Since a sharp wet front is approximated, the flow in the entire saturated region is equal to the boundary flow, i.e.,

$$g = g_{x=0} = \frac{dW}{dt} = \frac{A}{2\sqrt{t}} \tag{2.21}$$

As shown above, the capillary flow is driven by the pressure difference over a meniscus. The magnitude of this pressure gradient is, among other things, a function of the structural properties, i.e. the geometry of the liquid-vapour menisci present in the porous medium. Thus, the correct driving potential is the pressure gradient caused by the meniscus. It is assumed that the same pressure gradient is acting in all pores irrespectively of their size and shape. Thus, the parameter $(1/r_1 + 1/r_2)$, where r_1 and r_2 are the principal radii of the meniscus in two orthogonal directions, is assumed to be the same for all menisci in all pores. A basic weakness of the simple capillary suction theory is this; it assumes that moisture transport take place as a moving boundary. Therefore other theories have been developed. Besides, in a real material of a certain thickness there will be a combined liquid and vapour transport with a moisture front that is not completely sharp.

In soil science, the one-dimensional capillary flow is often described by an equation similar to Darcy's law. The driving potential used is the soil water potential Ψ, which is proportional to the pressure (Hall 1994):

$$g = -K(u)\frac{\partial \Psi}{\partial x} \tag{2.22}$$

where $K(u)$ is the unsaturated permeability. Ψ is the energy required to transfer a unit weight of liquid from the porous material to a reservoir of the same liquid at the same temperature and elevation. The units of Ψ can be [J/kg] (Nielsen et al. 1986) or [m] (Hall 1994). In the latter case, Ψ expresses the height to which a unit weight of the liquid will rise at equilibrium.

The soil water potential Ψ can be divided into the following parts (Nielsen et al. 1986):

$$\Psi = \sum \Psi_i = \Psi_P + \Psi_s + \Psi_e + \Psi_z \tag{2.23}$$

where

Ψ_P is the pressure potential;
Ψ_s is the solute potential;
Ψ_e is the electrochemical potential;
Ψ_z is the gravitational potential.

The pressure potential Ψ_P is applied to both the saturated and the unsaturated zone. In the unsaturated zone Ψ_P represents the capillary potential; in the saturated zone it represents

the applied pressure. The solute potential depends on the solute concentration. The electrochemical potential depends on the interaction of the soil particles and the solute. The solute potential and the electrochemical potential can often be neglected (Jonasson 1991).

Another approach for treating capillarity is to use Darcy's law with the pore water pressure P_ℓ [Pa] as the driving potential:

$$g = -D_\ell \frac{\partial P_\ell}{\partial x} \tag{2.24}$$

where the transport coefficient D_ℓ [kg/(m·s·Pa)] is a function of pore water pressure P_ℓ. In three dimensions the equation becomes:

$$g = -D_\ell \nabla P_\ell \tag{2.25}$$

The pore water pressure P_ℓ [Pa] is here defined as:

$$P_\ell = P_{atm} - P_{cap} \tag{2.26}$$

In Eq. 2.26 the atmospheric pressure P_{atm} is normally negligible. It is therefore often omitted:

$$P_\ell = -P_{cap} \tag{2.27}$$

2.2.3 Total moisture transport - Isothermal conditions

When calculating the moisture distribution, it is advantageous to have only one equation with one single transport coefficient that describes the total moisture transport in both vapour and liquid phases. Moreover, it is difficult to distinguish between vapour and liquid transport while measuring the moisture transport coefficients. Therefore, one equation with one transport coefficient is preferred.

If the assumptions contained within Eq. 2.12 and Eq. 2.25 are valid (i.e. the moisture flow is linearly proportional to the gradient of vapor pressure and pore water pressure) then the total transport can be described (here, in one dimension) by:

$$g = -\delta_p \frac{\partial p_v}{\partial x} - D_\ell \frac{\partial P_\ell}{\partial x} \tag{2.28}$$

At local equilibrium a relation exists between p_v and P_ℓ, as well as among all of the following moisture state variables: vapour content v [kg/m^3], vapour pressure p_v [Pa], relative humidity φ, pore water pressure P_ℓ [Pa], moisture content mass by mass u [kg/kg] and moisture content mass by volume w [kg/m^3]. The relation between u and w is:

$$w = u\rho \tag{2.29}$$

where ρ is the dry bulk density [kg/m^3]. The state variables φ, v, and p_v are related to each other by:

$$\varphi = \frac{v}{v_s} = \frac{p_v}{p_s} \tag{2.30}$$

where the index *s* refer to saturation. Both the vapour content and the vapour pressure at saturation are dependent on the temperature.

The general gas law relate the vapour content to the vapour pressure:

$$p_v = \frac{RT}{M_w} \cdot v \tag{2.31}$$

A relation between the pore pressure, the saturation vapour pressure and the relative humidity is given by Kelvin's equation:

$$P_\ell = p_s(T) + \frac{RT\rho_w}{M_w} \cdot \ln\varphi \tag{2.32}$$

The saturation vapour pressure p_s is normally negligible. It is often omitted in Eq. 2.32:

$$P_\ell = \frac{RT\rho_w}{M_w} \cdot \ln\varphi \tag{2.33}$$

where

R is the gas constant (8.314 J/(mol·K));
M_w is the molar weight of water (0.018 kg/mol);
ρ_w is the density of water [kg/m^3].

The moisture contents u and w are related to the relative humidity φ by the sorption isotherm (moisture content versus RH) and to the pore pressure P_ℓ by a water retention curve (moisture content versus capillary pressure).

According to Claesson (1993), the moisture state in a porous material can be characterised by three independent state variables; the total air pressure, the temperature and any of v, p_v, φ, P_ℓ, u or w. If the total air pressure is assumed to be constant, there will be only two independent state variables. At isothermal conditions there will be only one independent state variable, i.e. any of v, p_v, φ, P_ℓ, u or w. Since there is a unique relation between p_v and P_ℓ, Eq. 2.28 can be rewritten, at isothermal conditions:

$$\frac{\partial P_\ell}{\partial x} = \frac{\partial P_\ell}{\partial p_v} \cdot \frac{\partial p_v}{\partial x} = \frac{RT\rho_w}{M_w} \cdot \frac{1}{p_v} \cdot \frac{\partial p_v}{\partial x} \tag{2.34}$$

This leads to:

$$g = -\delta_p \frac{\partial p_v}{\partial x} - D_\ell \frac{RT\rho_w}{M_w} \cdot \frac{1}{p_v} \cdot \frac{\partial p_v}{\partial x} = -D_{new} \frac{\partial p_v}{\partial x} \tag{2.35}$$

where the "new" moisture diffusivity D_{new} is:

$$D_{new} = \delta_p + D_\ell \frac{RT\rho_w}{M_w} \cdot \frac{1}{p_v} \tag{2.36}$$

Generally Eq. 2.35 can be written:

$$g = -D_\phi \frac{\partial \phi}{\partial x} \tag{2.37}$$

where D_ϕ is the moisture diffusivity, which is dependent on the moisture content, and ϕ is any of the moisture state variables v, p_v, φ, P_ℓ, u or w. Moisture balance requires:

$$\frac{\partial w}{\partial t} = -\frac{\partial}{\partial x}(g) = \frac{\partial}{\partial x}\left(D_\phi \frac{\partial \phi}{\partial x} \right) \tag{2.38}$$

which in three dimensions becomes:

$$\frac{\partial w}{\partial t} = \nabla \cdot \left(D_\phi \nabla \phi \right) \tag{2.39}$$

Equations 2.37, 2.38 and Eq. 2.39 are valid at isothermal conditions and at local equilibrium since there are unique relations among all these state variables. It is not obvious, however, that there is a local equilibrium in the material in transient cases. The rate of the phase change in nonequilibrium thermodynamics is considered to be proportional to the difference between the thermodynamic potentials of each phase (Daian 1989). In transient transport processes the liquid- and vapour phases will consequently not be in local equilibrium as, for an example, Kelvin's equation presupposes.

The advantage of Equations 2.37, 2.38 and Eq. 2.39 is that the potential ϕ can be chosen to fit a special application or measurement. Relative humidity or moisture content are often natural choices since these potentials are directly measurable. But there are also disadvantages to using an arbitrary potential ϕ. For example, the equation is not pedagogically clear, so one might be erroneously led to believe that ϕ is the correct driving potential.

At isothermal conditions it is also possible to choose a flow potential, for which the moisture diffusivity is always equal to 1. This potential is called *Kirchhoff's flow potential*. When both measuring techniques and the numerical calculations are considered, the use of Kirchhoff's flow potential has turned out to be advantageous (Arfvidsson 1994). Kirchhoff's flow potential ψ [kg/(m·s)] is defined by:

$$\psi = \psi_{ref} + \int_{w_{ref}}^{w} D_\phi \, d\phi \tag{2.40}$$

i.e.

$$\frac{d\psi}{d\phi} = D_\phi \tag{2.41}$$

The three-dimensional moisture flow is described by:

$$g = -\nabla \psi \tag{2.42}$$

In one dimension the flow is:

$$g = -\frac{\partial \psi}{\partial x} \tag{2.43}$$

ψ_{ref} is the reference value at a moisture content $w = w_{ref}$ which can be chosen arbitrarily. The moisture balance equation expressed with Kirchhoff's flow potential in three and one dimensions, respectively, becomes:

$$\frac{\partial w}{\partial t} = \nabla \cdot (\nabla \psi) \tag{2.44}$$

$$\frac{\partial w}{\partial t} = \frac{\partial^2 \psi}{\partial x^2} \tag{2.45}$$

or:

$$C_\psi \frac{\partial \psi}{\partial t} = \nabla \cdot (\nabla \psi) \tag{2.46}$$

$$C_\psi \frac{\partial \psi}{\partial t} = \frac{\partial^2 \psi}{\partial x^2} \tag{2.47}$$

with the moisture capacity, C_ψ [s/m^2], described by (see Eq. 2.41):

$$C_\psi = \frac{dw}{d\psi} = \frac{1}{D_w} \tag{2.48}$$

2.2.4 Total moisture transport - Non-isothermal conditions

In solid wall structures, facades exposed to solar radiation, and other structures with large temperature gradients, the temperature gradient itself will impel moisture transport. In insulated multi-layer walls, most of the temperature gradient will occur over the insulation. The temperature gradients in other parts of the wall will be negligible.

If the temperature gradient is to be taken into account, there will be two independent state variables. In this case, the simplification done in section 2.2.3 is not possible (i.e. the vapour- and liquid flow in Eq. 2.28 must stay separated):

$$g = -\delta_p \frac{\partial p_v}{\partial x} - D_\ell \frac{\partial P_\ell}{\partial x} \tag{2.49}$$

All other state variables are known functions of p_v and P_ℓ. Here the transport coefficients δ_p and D_ℓ are functions of the two state variables used (i.e. δ_p and D_ℓ is a function of both P_ℓ and p_v). Although the state variables used in Eq. 2.49 are the physical determinants of diffusion and liquid flow, any other pair of independent state variables can be used. It is possible to change from one pair of state variables to another pair (Claesson 1993).

Künzel (1995) has presented an overview of different calculational methods used until now. The most commonly used pairs of state variables in these equations are (w, p_v), (p_v, P_ℓ) and (w, T). If, and in that case how, the corresponding transport coefficients have been measured for some materials is not clear in Künzels work. Künzel (1995) suggests the following balance equation:

$$\frac{\partial w_\ell}{\partial t} = \mathrm{div}\left(D_\varphi \nabla \varphi + \delta_p \nabla p_v\right) \tag{2.50}$$

where D_φ depends on the temperature and the moisture content, and δ_p depends on the temperature but not on the moisture content. According to Künzel (1995), the gradient of φ determines the liquid flow and the gradient of p_v determines the vapor flow. D_φ can be calculated from moisture distributions measured at various times in a material specimen undergoing capillary absorption. δ_p is obtained from cup-method measurements in the hygroscopic range. Thus two prerequisites for Eq. 2.50 are, that all moisture transport in the capillary absorption test occurs in liquid phase, and all moisture transport in the cup-method measurement occurs in vapor phase. This is, of course, to some extent an oversimplification. In spite of that, calculations (performed using Eq. 2.50) of moisture profiles during and after capillary suction on sandstone exposed to a varying climate, show an impressive agreement with measured values (Künzel 1995).

2.2.5 Two Phase flow and their interaction

In some applications it is desirable to distinguish between liquid flow and vapour flow. For example, dissolved chloride ions are transported by convection in the liquid phase but not within the vapour phase. In order to separate the flow of these two different phases, each phase needs its own equation that describes the transport. Moreover, an equation that describes the balance between the two phases is needed. The following reasoning is based on Johannesson (1996).

If the mathematical formulations describing vapour transport and liquid transport used in Eq. 2.13 and Eq. 2.24 are correct, the one-dimensional balance equations become:

$$\frac{\partial w_v}{\partial t} = \frac{\partial}{\partial x}\left(\delta_p \frac{\partial p_v}{\partial x}\right) \tag{2.51}$$

and

$$\frac{\partial w_\ell}{\partial t} = \frac{\partial}{\partial x}\left(D_\ell \frac{\partial P_\ell}{\partial x}\right) \tag{2.52}$$

Here, w_v is the vapour content mass per volume material [kg/m^3] and w_ℓ is the liquid content mass per volume material [kg/m^3]. The sum of the two phases consequently is the total moisture content w:

$$w = w_v + w_\ell \tag{2.53}$$

During a water transport process there will always be an evaporation or condensation at the water menisci. Thus, there will be a phase transformation between the vapour- and liquid phases. The equations that describe the two phase flow are:

$$\frac{\partial w_v}{\partial t} = \frac{\partial}{\partial x}\left(\delta_p \frac{\partial p_v}{\partial x}\right) + \hat{w}_v \tag{2.54a}$$

and

$$\frac{\partial w_\ell}{\partial t} = \frac{\partial}{\partial x}\left(D_\ell \frac{\partial P_\ell}{\partial x}\right) + \hat{w}_\ell \tag{2.54b}$$

where

$\hat{w}_v$ is a function describing the rate of water transformed from liquid to vapour [kg/(m^3·s)];

$\hat{w}_\ell$ is a function describing the rate of water transformed from vapour to liquid [kg/(m^3·s)].

The relation between $\hat{w}_v$ and $\hat{w}_\ell$ is:

$$\hat{w}_v = -\hat{w}_\ell \tag{2.55}$$

Consequently, the equations needed to describe the two phase flow are:

$$\frac{\partial w_v}{\partial t} = \frac{\partial}{\partial x}\left(\delta_p \frac{\partial p_v}{\partial x}\right) + \hat{w}_v \tag{2.56a}$$

$$\frac{\partial w_\ell}{\partial t} = \frac{\partial}{\partial x}\left(D_\ell \frac{\partial P_\ell}{\partial x}\right) - \hat{w}_v \tag{2.56b}$$

In the general three-dimensional case we have:

$$\frac{\partial w_v}{\partial t} = \nabla \cdot \left(\delta_p \nabla p_v\right) + \hat{w}_v \tag{2.57a}$$

$$\frac{\partial w_\ell}{\partial t} = \nabla \cdot \left(D_\ell \nabla P_\ell\right) - \hat{w}_v \tag{2.57b}$$

Besides these two equations, a third equation describing the phase transformation between the liquid and vapor flow is needed.

$$\hat{w}_v = f(w_v, w_\ell, \text{grad}(w_v), \text{grad}(w_\ell), T, \text{pore geometry}, \ldots) \quad (2.58)$$

Even though it sometimes is desirable to distinguish between liquid and vapor flow, it is impossible to measure the phase transformation (evaporation and condensation at the water menisci) with the measuring techniques available today. The same is also true for the two "clean" transport coefficients δ_p and D_ℓ. The transport coefficients obtained always describe the total moisture transport, since only the total moisture transport can be measured. Therefore, the coefficients in the different processes must be estimated. So, the use of Equations 2.56, 2.57, and 2.58 is limited. The equations can, however, be of use when parameter studies are done. In the future, new measuring techniques that can distinguish between the two phases might be available.

2.2.6 Pore space models

It would be desirable to have a universal model from which the capillary transport or the transport coefficient could be evaluated. Such a model would be independent of the material, and be based on simple geometrical properties such as the porosity, the specific area, and the pore shape. This is probably not possible, since the pore system is always extremely complex and difficult to quantify geometrically. Besides it is different in each material.

Many proposals of different pore space models have been put forward. These models are more or less useful for modeling capillary transport in different types of materials. They can be divided in one-, two- and three-dimensional models. The one-dimensional models require co-linear flow only; in the two-dimensional models the flow takes place in a plane; and in the three-dimensional models the transport can occur in three-space. Since capillary transport always takes place in three dimensional networks, the three-dimensional models are, of course, the most suitable.

Since the pore system in a porous material is very complex and irregular, the necessary approximations made in the pore space model will decrease the usability and reliability of the model. Van Brakel (1975) has enumerated and classified almost all proposed pore space models. He writes: "In order to remove too optimistic ideas about the use of pore space models, all models are checked against the phenomena of capillary rise (e.g. water in sand). The predictions of the models regarding statics and dynamics of capillary rise are compared with the experimental facts and it appears that none of the models can give even a qualitative description of the observed phenomena".

2.2.7 Required measurements

As shown above, there exist several different models to describe moisture transport in porous materials. It is important to keep in mind, the mathematical model in which the measured data will be used. For example, transport coefficients measured under isothermal conditions cannot automatically be used in non-isothermal models. If the moisture content w and the temperature T are used as state variables in the non-isothermal model, the transport coefficients will be $D_w(w, T)$ and $D_T(T, w)$, respectively. In this case, measurements must be performed at varying moisture contents and moisture gradients, at different temperature levels and temperature gradients.

It should also be noted that the choice of state variables influences the transport coefficients, e.g. δ_p in Eq. 2.49 is not equal to δ_p in Eq. 2.50. If the state variables (p_v, P_ℓ) (used in Eq. 2.49**)** are changed to a new couple of the state variables (φ, p_v), the "new" $\delta_p(\varphi, p_v)$ becomes (Claesson 1993):

$$\delta_p(\varphi, p_v) = \delta_p(p_v, P_\ell) + D_\ell(p_v, P_\ell)\frac{\partial P_\ell}{\partial p_v} \tag{2.59}$$

Thus, the measured transport coefficients are closely connected to the theoretical physical model to which they are applied and to the potential used.

2.3 Moisture fixation

Water can be bound in porous materials in several different ways, both physical and chemical. In contact with moist air, water molecules are bound physically to the surfaces of the pore system until an equilibrium with the humidity of the ambient air is reached. Chemically bound water only exists in some materials, such as cement based materials, in which some of the mixing water is bound in the cement gel. Such water is not lost until the gel is dried above 105°C.

Water in porous materials is often classified as evaporable or non-evaporable. Normally, evaporable water is water lost by drying at 105 degrees C. It is often assumed that the physical water is evaporable and the chemically bound water is non-evaporable. According to Ahlgren (1972) this classification is somewhat ambiguous. That is, different methods of evaporating water exist, which give different results. The classification in evaporable and non-evaporable water is, however, practical and probably accurate enough for most applications.

Physically bound water can be bound by *adsorption* and *capillary condensation.* Adsorbed water molecules are bound to the pore surface by van der Waal forces. At equilibrium the amount of adsorbed water per square meter of pore surface is a function of the temperature and the relative humidity of the ambient air. There is never a static condition. As some water molecules leave the pore surface, other water molecules become attached. At equilibrium, the number of molecules leaving is the same as the number becoming bound to the surface.

Capillary condensed water molecules are condensed on curved water menisci that are formed in small pores and other narrow spaces. A relation exists between the relative humidity φ when condensation take place and the principal radii of the curvature of the meniscus in two orthogonal directions, r_1 and r_2. A combination of Eq. 2.5 and Eq. 2.33 gives:

$$\ln\varphi = -\frac{M_w}{RT\rho_w}\cdot\sigma\cos\theta\cdot\left(\frac{1}{r_1}+\frac{1}{r_2}\right) \tag{2.60}$$

Salts dissolved in pore water lower the relative humidity at which capillary condensation takes place. This effect is similar to that occurring for a curved water surface (i.e., the material will absorb more water from the ambient air if salt is present in the pore water).

In the hygroscopic range, the relation between the moisture content of the ambient air and the moisture content of the material is given by the sorption isotherms. In the superhygroscopic range, the relation is given by the retention curves. For many materials this relation is different, depending on whether equilibrium is reached by absorption or desorption. In the sorption isotherm the moisture content (in most cases expressed by u or w) is plotted against the relative humidity; and in retention curves the moisture content is plotted against the capillary pressure.

3 Methods of measuring the moisture diffusivity

3.1 Introduction

In the hygroscopic range (up to approximately 98% relative humidity) several well documented measurement methods are available, see e.g. (Nilsson 1980) and (Hedenblad 1993). The most frequently used method is probably the cup method. On materials with little or no superhygroscopic range (i.e. with pore radii smaller than approximately 50 nm), the cup method alone is sufficient enough to measure the moisture diffusivity D_w. This is due to the fact that these materials are already water saturated, at equilibrium with approximately 98% relative humidity. Examples of such materials are concrete with low water to cement ratio, granite, etc. In (Hedenblad 1996) the moisture permeability δ_v and the Kirchhoff's flow potential ψ for a large quantity of different building materials are reported. Values were measured by the cup method in the hygroscopic range at isothermal conditions. The cup method is also described in detail by Hedenblad (1996).

On materials with a coarse pore system (e.g. some natural sandstones, bricks, lime silica bricks, and aerated autoclaved concrete) the cup method measurements must be supplemented by some other method. As an example, the degree of capillary saturation of the natural sandstone studied in this report is only 8 to 9% at an equilibrium with 97% relative humidity. Thus, more than 91 to 92% of the pores are in the superhygroscopic range. For these materials the sorption isoterm must also be supplemented by measurements from a water retention curve. Such measurements are also described and reported by e.g. Krus (1995) and Kießel et al. (1993).

In this chapter some different methods of measuring the moisture diffusivity at high moisture levels will be shortly presented.

3.2 Methods based on profiles during a transient moisture uptake or redistribution

3.2.1 Theoretical evaluation of moisture profiles

The moisture diffusivity can be calculated from the moisture profile measured at various times after start of water uptake or start of moisture redistribution. The profiles are measured on specimens that are absorbing free water from their boundary, or from the redistribution process occurring when the absorption process is interrupted. Some of the possible methods for measuring moisture profiles are described below. Two of the most common methods used are the Boltzmann transformation method and the Profile method. They are described by de Freitas et al. (1995).

The Boltzmann transformation method necessitates a step change of the boundary moisture level ($w(x, 0) = w_{in}$; $w(0, t)$ = constant) and is valid only for a semi-infinite volume. That is, with the Boltzmann transformation method the moisture diffusivity can only be calculated from absorption profiles. The material must also have a linear correlation between mass flux and square root of time. The moisture diffusivity D_w is calculated by (see Figure 3.1):

$$D_w(w_2) = -\frac{1}{2 \cdot \frac{\partial w}{\partial U}} \cdot \int_{w_{in}}^{w_2} U \, dw \tag{3.1}$$

where

w is the moisture content [kg/m^3];
U is a the Boltzmann's variable [m/s^{½}] defined by

$$U = \frac{x}{\sqrt{t}} \tag{3.2}$$

The Profile method can be used on profiles measured during both the absorption- and the redistribution process. The moisture diffusivity is expressed as a function of an average moisture profile curve between two measured profiles (see Figure 3.1):

$$D_w = -\frac{1}{dt} \cdot \frac{\int_{x=x_0}^{x=\ell} \left(w_{t+dt}(x) - w_t(x) \right) dx}{\frac{\partial w_0}{\partial x_0}} \tag{3.3}$$

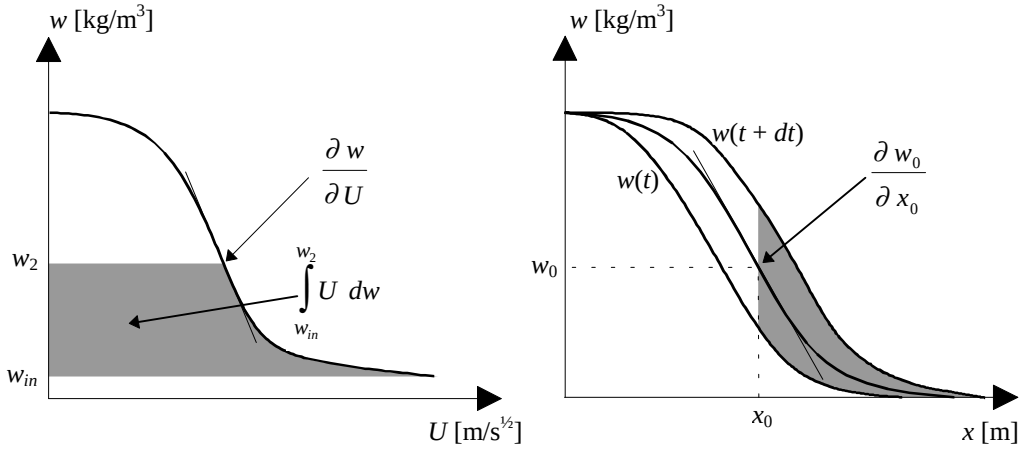

Figure 3.1 Principle of the Boltzmann method (left) and the Profile method (right).

3.2.2 Slice-dry-weigh -method

Whenever the moisture profile is to be measured, a specimen is rapidly sliced into discs that are weighed, dried, and weighed again. The water in the disc evaporates during the drying and the water content in mass by mass can be calculated from the weight loss. The drying procedure can be executed in several different ways, depending on the material tested and their ability to resist heat. The quickest and most common way is to use an oven at 105°C. Materials that cannot resist heat can, for example, be dried in an exsiccator with some drying agent like silica gel or sulfuric acid. This procedure is rather time consuming.

The method is destructive and one specimen is destroyed every time the moisture profile is measured. The slicing might be difficult for some materials. A saw cannot be used since heat is generated or water added during the sawing. Thus, the specimen must be sliced through splitting. With splitting, it is difficult to get the crack perfectly parallel to the surface exposed to water. An error in measuring the x-coordinate of the disc is therefore easily obtained. It might also be difficult to split the specimen into discs thin enough to evaluate a very steep water front. Another disadvantage of this method is that a considerable number of specimens must be used, since the method is destructive. It might even be impossible to get a number of specimens high enough if they have to be taken from an existing building. This method is suitable when water and non-volatile fluids are used for the absorption experiment, but it is unsuitable for a volatile fluid, as this will evaporate from the disc during the splitting process.

This is the most accurate method, provided that the slicing can be done in an accurate way. It is the most accurate method because the actual amount of water in the specimen is measured. Therefore, it should always be used to calibrate and verify all the other methods described below.

3.2.3 Electrical methods

Two non-destructive electrical methods are available. One is based on measuring the variation of electrical conductivity (resistance), and the other is based on measuring the variation of electrical capacitance. For most materials the electrical conductivity increases with increasing moisture content. For all materials the capacitance increases with the moisture content due to the high dielectric constant of water (Adamson et al. 1970). Both methods, especially the resistance method, are inexpensive.

The conductivity, or actually the electrical resistance, is measured between two electrodes in direct contact with the material. The water content is evaluated from the resistance measured using a calibration curve valid for the actual material. The calibration curve is obtained with rather time consuming and extensive calibration tests. The conductivity is influenced by factors other than the water content (e.g. salts, temperature, density, etc.). According to Wormald et al. (1969), the resistivity of a concrete with the same water content may vary up to 40% with change in the salt concentration of the pore water. The use of this method is therefore limited when any of these factors are varying. Conductivity measurements are mostly used on wood but have also been used on other materials. As an example, a conductivity measurement made on aerated autoclaved concrete with an accuracy on the moisture content of ±10% is presented by Sandin (1978). One possible way of avoiding the effect of salts is to measure the conductivity in a special sensor (e.g. a piece of wood) that is embedded in the material to be studied. The sensor can be protected from

salts in the material. After a certain time it will adopt the same moisture state as the material. A calibration curve for the sensor is required, however. This type of sensor can only be used when slow changes in the moisture state are to be measured. That is because it will take a relatively long time for the sensor to adopt the same moisture state as the material.

The capacitance method uses the tested material as a dielectric. According to Krus (1995), the dielectric constant of water is 10 to 40 times larger than that of a dry building material when the frequency is 1 GHz. In that way the change of the capacitance is a measure of the water content in the material used as the dielectric. The capacitance method is less influenced by salts in the pore water and by density differences in the material than the conductivity method. The capacitance method however requires a more complicated laboratory set up. According to Wormald, et. al. (1969), the accuracy of the capacitance method applied to concrete is ±0.25% of moisture content mass, per mass in the range 0-6.5%.

3.2.4 Gamma-ray attenuation

This is a non-destructive method. If two different gamma ray sources are used, both the water content and the density can be measured. The gamma rays (photons) interact with the orbital electrons in the material and are absorbed or scattered. The intensity of a narrow beam of gamma rays passing through a material can be expressed by (Nielsen 1972, Descamps 1990):

$$I = I_0 \mathrm{e}^{-\mu\rho x} \tag{3.4}$$

where

- I is the gamma ray intensity after passing through the material [counts/s];
- I_0 is the intensity without absorbing material [counts/s];
- μ is the mass absorption coefficient of the material [m^2/kg];
- ρ is the density of the material [kg/m^3];
- x is the thickness of the material sample [m].

In order to perform a measurement of the moisture profile, a gamma ray source and a detector are needed. The source can be buried in the material with the detector on the surface, or, more commonly, the specimen can be placed between the source and the detector. The source can consist of Am^{241}, Cs^{137} or Co^{60}. The detector is usually a scintillation crystal, e.g. a NaI crystal.

The gamma ray equipment must be calibrated against the specific material in question. The equipment is rather expensive. Gamma rays should not be used if the material structure changes in time (e.g. during the hydratation process of young concrete). The reason is that the hydration reduces the moisture content by transforming ”free water” to chemically bound water. During this process, the density of the concrete increases. According to Adamson, et. al. (1970), the accuracy of the gamma ray method applied to concrete is ±0.5% of moisture content mass, per unit of mass. A disadvantage of the gamma ray method is that special safety arrangements must be taken due to the radioactivity. Examples of results and laboratory set ups are shown in Quenard et al. (1989), Nielsen (1972) and Wormald et al. (1969).

3.2.5 Neutron radiography

Similar to gamma ray attenuation, neutron radiography is a non destructive method using radiation. In contrast to gamma rays, neutrons interact mainly with the hydrogen nuclei. The attenuation of a neutron beam, caused by scattering and absorption of the neutrons, will therefore be directly related to the total water content in the material. The intensity of a neutron beam passing through a specimen is described by an expression similar to Eq. 3.4 (Pel 1995):

$$I = I_0 \mathrm{e}^{-x\left(\mu_{mat}+\mu_w \cdot \varepsilon\right)} \tag{3.5}$$

where

I is the intensity of a neutron beam after passing through the material [counts/s];
I_0 is the initial intensity of the neutron beam [counts/s];
μ_{mat} is the macroscopic attenuation coefficient of the specific material [m^{-1}];
μ_w is the macroscopic attenuation coefficient of water [m^{-1}];
x is the thickness of the material sample [m];
ε is the water content volume by volume [m^3/m^3].

The coefficients μ_{mat} and μ_w are determined independently by measuring the neutron transmission through pure water, and through the dry material in question. During the test the specimen is placed between the neutron source and the detector. The neutron beam can be produced by a combination of boron and cadmium and the neutrons can be detected by a ^{3}He proportional detector (Pel 1995). When running a neutron radiography test safety arrangements must be taken and specially trained personnel are necessary. Results from measurements with neutron radiography on different materials and experimental arrangements are shown in Pel (1995), Adan (1995), Justnes et al. (1994), and Dawei et al. (1986).

3.2.6 Nuclear magnetic resonance

Nuclear magnetic resonance (NMR) is a non-destructive method. The accuracy of the water content measurement is approximately 0.5 to 0.1 vol.-% according to Kießel et. al. (1991). NMR has a spatial resolution of better than 1 mm according to Kopinga et al. (1994). With NMR, a distinction can also be made among free, physically bound and chemically bound water. Thus, NMR is a very well suited for measuring transient water movements in building materials. A primary disadvantage of NMR is that the equipment needed is rather expensive.

In an NMR measurement the number of hydrogen nuclei are ”counted”. A magnetic moment is associated with the intrinsic spin of the material’s hydrogen nuclei. In a NMR experiment an exterior permanent magnetic field is applied. When an electromagnetic field is applied perpendicular to the constant magnetic field, some energy is absorbed. The amount of energy absorbed is proportional to the number of hydrogen nuclei in the measurement volume. It is therefore a measure of the water content in the material tested. In addition to water, NMR is suitable for all fluids containing hydrogen atoms.

According to Kopinga et al. (1994), NMR offers better sensitivity than gamma-ray attenuation and neutron radiography. Unlike results from the gamma ray method, the NMR

results are directly related to the amount of hydrogen nuclei. In de Freitas et al., (1995), however, a comparison between gamma-ray attenuation and NMR revealed no significant difference in accuracy. An advantage of NMR compared to gamma-ray attenuation and neutron radiography is that no radioactivity is involved during the experiment. Examples of results from NMR measurements and laboratory arrangements are shown in e.g. Krus (1995), Pel (1995), Brocken et al. (1995), Kopinga et al. (1994) and Kießel at al (1991).

3.2.7 Computer tomography

The principle of computer tomography is to measure the intensity loss of a narrow beam of X rays passing through the specimen. The absorption is a measure of the density of the specific material in question. The magnitude of the absorption is measured with a so-called CT-value. The scale is calibrated against distilled water. By definition, water has a CT-value of 0. The absorption (CT-value) in air is -1000, which means that there is no absorption (100% less absorption). The absorption of X rays in concrete is 145-150% greater than the absorption in water. The CT-value of concrete consequently is 1450-1500. (Bjerkeli 1990). The difference in the CT-value between air and water is an indicator for measuring the water content in the material.

3.2.8 Microwave beam

Non destructive measurement of the moisture profile can be carried out with a microwave beam. Microwave attenuation is strongly influenced by the dielectric constant of the material (Adamson et al. 1970). The dielectric constant of water is 10 to 40 times higher than that of dry material.

During the measurement the specimen is placed between a transmitter and a receiver and the attenuation of the beam caused by the oscillation of the water molecules is measured. The magnitude of the attenuation corresponds to the water content of the tested material. The equipment must be calibrated against the specific material in question. If the power of the beam is too high, the temperature of the water in the material will strongly increase during the test. Moisture migration caused by the temperature gradient might therefore occur. This measuring technique and some results are in detail described in Volkwein (1993), Wittig et al. (1992) and Volkwein (1991).

3.2.9 Thermal conductivity

The thermal conductivity of a material increases with increasing moisture content. If the relation between the moisture content and the thermal conductivity is known for a certain material, the moisture content can be measured with this method.

The principle of the method is to generate a known amount of heat locally in the material and then measure the temperature vs. time curve at a certain distance from the heat source. This temperature curve is a measure of the thermal conductivity. Therefore, if the relation between the moisture content and the thermal conductivity is known, the moisture content can be calculated. The heat source will, however, generate a temperature gradient. This will influence the moisture flux and so the temperature gradient is a source of error. According to Vos (1965) is it possible to measure the moisture content with a precision of ±1 vol. %.

3.2.10 Thermal imaging

This is a simple method to determine the moisture distribution, or the distribution of volatile fluids. The principle is based on the decreasing temperature when liquids evaporate. The method is destructive and one specimen is used every time the moisture profile is to be measured. When the profiles are to be measured the specimen is split into two halves, perpendicular to the exposed surface. The temperature of the split surface is measured with an infrared camera. From the temperature distribution the moisture profile is evaluated. According to Sosoro et al. (1995), the moisture profile in a specimen with a constant cross-section over the depth can be calculated by:

$$\varepsilon(x) = \frac{\left(T_0 - T_s(x)\right)^2}{\frac{S}{V_{fl}} \cdot \int_0^{\ell} \left(T_0 - T_s(x)\right)^2 dx} \tag{3.6}$$

where

ε is the water content volume, per volume [m^3/m^3];
T_0 is the temperature of the surrounding air [K];
T_s is the surface temperature [K];
x is the co-ordinate in the direction of water transport [m];
S is the surface area exposed to fluid [m^2];
V_{fl} is the total absorbed test fluid [m^3];
ℓ is the specimen length [m].

Another method is to calibrate the measured temperature of the split surface against the temperature of split surfaces of well conditioned specimens. The calibration is performed on specimens of the specific material with different and known moisture contents. The measuring procedure and conditioning procedure must take place in a climate room with constant relative humidity and temperature, and the image must be taken at the same time after splitting the specimen. This conditioning procedure would be very time consuming, but the accuracy of the measured water content would probably be higher than the water content obtained with Eq. 3.6.

Profiles of different liquids and laboratory arrangements are described in Sosoro et al. (1995) and Sosoro (1995).

3.3 Other methods

3.3.1 Evaluating the moisture diffusivity from the sorption coefficient

There exist some methods to calculate the moisture diffusivity at high moisture levels from other moisture properties than the moisture profile. One such method employs the sorption coefficient. Two methods of evaluating the moisture diffusivity at high moisture levels from a series of capillary water uptake tests and results from these methods are described in detail in Chapter 5. Künzel (1995) suggests the following equation for calculating the moisture diffusivity D_w from the sorption coefficient:

$$D_w = 3.8 \cdot \frac{A^2}{w_{cap}^2} \cdot 1000^{\frac{w}{w_{cap}}-1} \tag{3.7}$$

where

A is the sorption coefficient [kg/(m^2·s^{½})];
w is the moisture content [kg/m^3];
w_{cap} is the moisture content at capillary saturation, defined in section 4.2.7 [kg/m^3].

In Eq. 3.7, the increase of the moisture diffusivity with increasing moisture content is approximated with an exponential function. The theory behind this approach is unclear. Perhaps it is purely empirical.

3.3.2 Evaluating the moisture diffusivity from steady state moisture profiles

The moisture diffusivity at high moisture levels can also be evaluated from moisture profiles at steady state. One method of this type will be described.

It is based on measurements of the relation between the moisture content and Kirchhoff's flow potential up to capillary saturation. It is described in Arfvidsson (1994) and Hedenblad (1993). Instead of measuring moisture profiles as they develop in the specimen during the transient water uptake, profiles are measured only after the flux has reached a steady state. The moisture profile can be measured by the "slice-dry-weigh" -method described in section 3.2.2. The moisture flow at steady state, $g_{t=\infty}$ must also be known. The profile can be measured in terms of degree of saturation or in terms of moisture content (mass per mass, or mass per volume). Relative humidity is not suitable at the high moisture levels occurring during capillary suction. In the following, the moisture content mass per volume w [kg/m^3] will be used. Using Kirchhoff's flow potential, Fick's law is

$$g = -\frac{\partial \psi}{\partial x} \tag{3.8}$$

Here Kirchhoff's flow potential is a function of the moisture content

$$\psi = \psi(w) \tag{3.9}$$

Consider steady state through a specimen $0 \le x \le \ell$. At $x = 0$ there is capillary saturation and at $x = \ell$ there is a constant value $w(\ell)$. The steady state moisture profile is $w = w(x)$ and the flux $g_{t=\infty}$. Then we have:

$$g_{t=\infty} = -\frac{d}{dx}\left[\psi\left(w(x)\right)\right] \tag{3.10}$$

Integration from 0 to x gives

$$g_{t=\infty} \cdot x = -\psi\left(w(x)\right) + \psi\left(w_{cap}\right) \tag{3.11}$$

or

$$\psi(w) = \psi(w_{cap}) + \left(-g_{t=\infty}\right) \cdot x \tag{3.12}$$

With Eq. 3.12 the stepwise relation $\psi(w)$ now can be calculated.

Example (notations according to Figure 3.2): At steady state the difference of Kirchhoff's flow potential between two points, $\Delta\psi$, within a distance of Δx in a homogenous material is described by Eq 3.11:

$$\Delta\psi = -g_{t=\infty} \cdot \Delta x \tag{3.13}$$

The difference in the Kirchhoff flow potential through the whole specimen ($\Delta x_1 = x_1 = \ell$) is calculated by

$$\Delta\psi_1 = \psi(w_1) - \psi(w_{cap}) = -g_{t=\infty} \cdot x_1 \tag{3.14}$$

With $\psi_{ref} = \psi(w_1) = 0$, $\psi(w_{cap})$ is calculated (ψ_{ref} can be chosen arbitrary):

$$\psi(w_{cap}) = g_{t=\infty} \cdot x_1 \tag{3.15}$$

The difference in the Kirchhoff flow potential, from the exposed surface to the level $x = x_2$ ($\Delta x_2 = x_2$), is calculated by (see Figure 3.2)

$$\Delta\psi_2 = \psi(w_2) - \psi(w_{cap}) = -g_{t=\infty} \cdot x_2 \tag{3.16}$$

According to Eq. 3.15 $\psi(w_{cap}) = g_{t=\infty} \cdot x_1$; That is:

$$\psi(w_2) = g_{t=\infty} \cdot \left(x_1 - x_2\right) \tag{3.17}$$

A stepwise linear relation $\psi(w)$ can accordingly be calculated by

$$\psi(w_1) = \psi_{ref} = 0 \tag{3.18a}$$

$$\psi(w_2) = g_{t=\infty} \cdot \left(x_1 - x_2\right) \tag{3.18b}$$

$$\psi(w_3) = g_{t=\infty} \cdot (x_1 - x_3) \tag{3.18c}$$

$$\vdots$$

$$\psi(w_{cap}) = g_{t=\infty} \cdot x_1 \tag{3.18N}$$

A disadvantage of this method is that it will take a considerable time for the specimen to reach steady state. It is also difficult to use the method on materials with very steep profiles. Furthermore, the surface exposed to water will reach a higher moisture content than that corresponding to capillary saturation. This gradual water absorption exceeding w_{cap} is not a flow process described by Fick's law. Therefore, the part of the profile with $w > w_{cap}$ can not be used when calculating the relation between Kirchhoff's flow potential and water content. The process going on at the surface part is a process in which the air enclosed in the specimen pores is solved in the pore water. This process can probably be described with a source term $f(w)$ in the moisture balance equation:

$$\frac{\partial w}{\partial t} = \frac{\partial^2 \psi}{\partial x} + f(w) \tag{3.19}$$

It must be observed that this gradual water absorption above w_{cap} is not a moving boundary but a process going on simultaneously across a considerable pore volume, e.g. (Fagerlund 1993). Only the part of the specimen with a water content below w_{cap} should be used when calculating $\psi(w)$, see Figure 3.3.

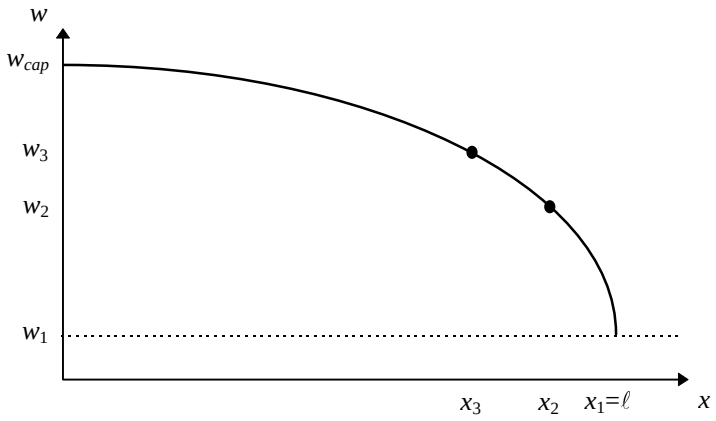

Figure 3.2 The moisture profile at steady state through a specimen with a length ℓ and with one boundary exposed to water (capillary saturation on the surface) and the other boundary exposed to a constant climate corresponding to w_1.

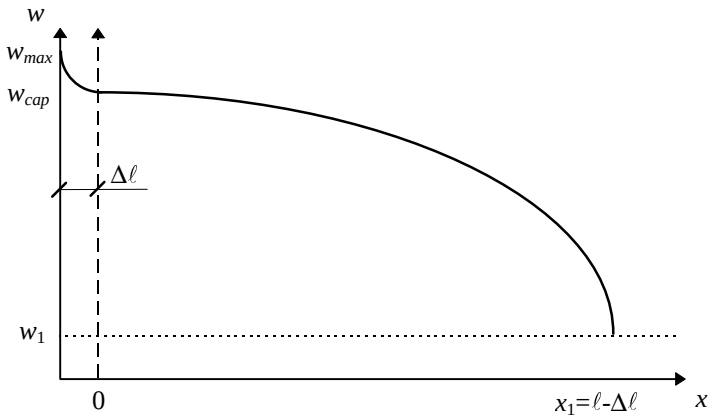

Figure 3.3 Only the part of the specimen with a water content below w_{cap} can be used when calculating ψ(w). The x-axis is moved a distance Δx so that the used fictive length become ℓ - Δℓ.

4 Experiments

4.1 General

The purpose of the experimental work was to find a relation between the water sorption coefficient, A [kg/(m^2·s^{½})] (defined by Eq. 4.11), and the initial moisture content in the specimens before testing, w_{in} [kg/m^3]. This relation $A(w_{in})$ is then used to calculate the moisture diffusivity D_w [m^2/s] and Kirchhoff's flow potential ψ [kg/(m·s)](see Chapter 5). In order to obtain the relation $A(w_{in})$, the specimens were conditioned to different desired initial water contents, in both the hygroscopic and the superhygroscopic ranges. The water sorption coefficient was then measured by letting the pre-conditioned specimen suck water. The amount of absorbed water was recorded on-line, automatically. A sorption isotherm and a water retention curve were also obtained when conditioning the specimens. In order to determine the water content mass per volume, the density was measured on each and every specimen. From this measurement the specimen volume, porosity and compact density were also obtained. The results in this chapter are mainly taken from Janz (1995).

4.2 Material and methods

4.2.1 Material

All experiments are made on a sedimentary calcareous sandstone named Uddvide. The stone is from a quarry on the island of Gotland, Sweden. The colour of the stone is homogeneously light grey. Gotland sandstone is one of the dominant materials in historical buildings in the Baltic region (Lindborg 1990). Since Gotland sandstone is soft and therefore easy to work, it was often used in sculptural decorations and facings on churches, castles and private dwellings during the seventeenth and eighteenth centuries (Wessman 1996).

The porosity of Uddvide sandstone is approximately 23% and the density 2059 kg/m^3, see section 4.2.7 and section 4.3.2. Thin section microscopy of the stone shows that it almost entirely contains quartz grains glued together by calcite with empty spaces constituting the porosity, see Figure 4.1. The size of the grains is according to Wessman and Carlsson (1995) 0.1-0.2 mm.

4.2.2 Experimental arrangement

In order to be able to perform a rapid conditioning to the desired initial water content, it was desirable to keep the specimen as small as possible. At the same time the specimen had to be big enough in the direction of the water transport, so that it could be considered as a semi-infinite volume at the beginning of the capillary water uptake test. In order to find a suitable length of the specimen, a pre-study was carried out with varying specimen length. This study resulted in specimens with lengths of approximately 25 mm and with a diameters of approximately 64 mm.

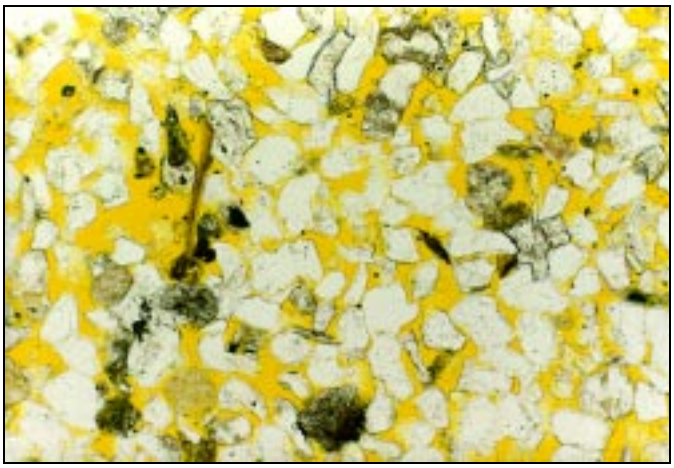

Figure 4.1 Thin section microscopy of Uddvide sandstone. The size of the picture corresponds to 1.2 x 0.8 mm in natural scale. The yellow fields are pores filled with epoxy (Wessman and Carlsson 1995).

In the hygroscopic range the sorption isotherm was determined on the basis of the weight of the specimens. These specimens were conditioned in climate boxes before start of the capillary water uptake test. The specimens were conditioned until a state of equilibrium was established between the specimen and the climate in the climate boxes. These measurements were also supplemented by measurements on specimens, that were used only for the determination of the sorption isotherm. These specimens have the same diameter as the specimens used for the capillary water uptake test, but they have a thickness of approximately 4 mm.

In the hygroscopic range the specimens were conditioned both by absorption from a completely dry state and desorption from a saturated state. For the capillary water uptake test 3 specimens were conditioned by absorption and 3 specimens conditioned by desorption per climate (i.e. totally 6 specimens per climate). Two specimens for determination of the sorption isotherms were conditioned by absorption and 2 specimens were conditioned by desorption per climate (i.e. totally 4 specimens per climate). In total, 8 climate boxes were used (see section 4.2.3). This gives 48 specimens used for the capillary water uptake test (24 by absorption and 24 by desorption) and 32 specimens used for the determination of the sorption isotherm only (16 by absorption and 16 by desorption).

In the superhygroscopic range the specimens were conditioned by pressure in pressure plate cells. All conditioning was done by desorption from saturated condition. Three specimens per pressure (initial moisture content) were used.

The methods used for conditioning the specimens both in the hygroscopic range and the superhygroscopic range were chosen to prevent moisture gradients over the body of the specimens. But, if the two methods of evaluating the moisture diffusivity from the relation $A(w_{in})$ presented in Chapter 5 should be more extensively used, a more rapid method of conditioning must be used. Therefore a an additional rapid method of preconditioning the specimens has been tried on 15 specimens.

4.2.3 Conditioning in the hygroscopic range

Three specimens per relative humidity (RH) were conditioned by absorption and three by desorption in the hygroscopic range. Before conditioning the specimens, the dry weight was obtained by drying them for 7 days at 105°C. The specimens were cooled afterwards in an exsiccator using silica gel. The specimens were weighed on a balance with a resolution of 1 mg. The specimens to be used for desorption were water saturated for one day and then placed in the climate boxes. The specimens to be used for absorption were placed in climate boxes immediately after weighing. Initial moisture gradients over the specimen body were prevented by the conditioning method used while the specimens were conditioned through absorption or desorption.

Eight different climate boxes were used for conditioning the specimens. The boxes were placed in a room with a temperature of approximately 20°C. Different saturated salt solutions were used to obtain the desired relative humidity in the climate boxes. The air in the boxes were circulated by a fan. The relative humidity of the salts used were: 11% (LiCl), 33% ($MgCl_2$), 59% (NaBr), 75% (NaCl), 85% (KCl), 91% ($BaCl_2$), 94.5% (KNO_3) and 97,6% (K_2SO_4). The specimens were left in the boxes until no change in weight were observed over a period of 28 days. The moisture content expressed as mass per mass, u_{in} and the moisture content expressed as mass per volume, w_{in} are calculated by:

$$u_{in} = \frac{m_{in} - m_0}{m_0} \tag{4.1}$$

$$w_{in} = u_{in}\,\rho \tag{4.2}$$

where

m_{in} is the mass of the specimen after conditioning (equal to the initial mass at the beginning of the capillary water uptake test) [kg];
m_0 is the dry weight [kg];
ρ is the density (see section 4.2.7) [kg/m^3].

4.2.4 Conditioning in the superhygroscopic range

In the superhygroscopic range the specimens were conditioned in so-called extractors. Two different types of extractors were used; a pressure plate extractor for pressures up to 15 bar and a pressure membrane extractor for pressures between 15 and 100 bar. The function of the two types of extractors is the same. The specimens together with the porous ceramic plate/cellulose membrane on which the specimen is placed are saturated with water. This is done by letting the specimens and the ceramic plate/cellulose membrane suck water for approximately 24 hours. The specimens are then placed on the porous ceramic plate, or cellulose membrane and mounted in the pressure vessel. Capillary forces in the pore system of the ceramic plate/cellulose membrane are able to stand up to the maximum dimensioned applied pressure in the vessel, see Figure 4.2. The maximum air pressure that any given ceramic plate/cellulose membrane can stand, before air passes through the pores, is determined by the diameter of the pore. When the pressure is raised, water is forced out of the specimen, through the saturated ceramic plate/cellulose membrane and out of the vessel, (see Figure 4.3.)

The equipment used for conditioning the specimens was originally designed for testing soil samples. In order to use the equipment on solid materials, and still get a good hydraulic contact between the specimens and the ceramic plate/cellulose membrane, saturated kaolin clay is used to perfectly join the specimen to the ceramic plate/cellulose membrane. Between the kaolin and the ceramic plate/cellulose membrane is a cloth. It is placed to prevent the kaolin from penetrating the specimen. This set-up was originally designed by Krus and Kießl and is presented in e.g. Krus and Kießl (1991) and Krus (1995).

When the ceramic plate/cellulose membrane with specimens placed upon them is mounted in the vessel and the desired overpressure is applied, the conditioning starts. The excess water in the specimen is forced out of the specimen through the cloth, kaolin clay, ceramic plate and out of the vessel. The excess water that flows out of the outflow tube, see Figure 4.3, is collected in a burette. The conditioning is to be considered completed when no outflow can be measured over a day. This procedure takes about 1 to 2 weeks depending on the pore size distribution of the specimen and the over-pressure applied. The relation between the capillary pressure and the applied air pressure (overpressure) is:

$$P_{cap} = P_{air} \tag{4.3}$$

Sometimes is it convenient to use the pore water pressure P_ℓ, instead of capillary pressure. The relation between pore water pressure and the capillary pressure is given by:

$$P_\ell = P_{atm} - P_{cap} \tag{4.4}$$

where the atmospheric pressure P_{atm} [Pa] normally is negligible and omitted.

Three different ceramic plates with different pore systems (pore diameter) are used. They are dimensioned to stand up to 1, 3 and 15 bar overpressure, respectively. The 1 bar ceramic plate has the largest pore diameter and the 15 bar ceramic plate the smallest. The conditioning procedure is quicker when larger pores are used in the plate. The cellulose membrane is capable of withstanding up to 100 bar.

A relation among the pore pressure, P_ℓ [Pa], the saturation vapour pressure, p_s [Pa], and the relative humidity, φ [-], is given by the Kelvin equation:

$$P_\ell = p_s(T) + \frac{RT\rho_w}{M_w} \cdot \ln\varphi \tag{4.5}$$

The saturation vapour pressure p_s is normally negligible, and it is often omitted in Eq. 4.5:

$$P_\ell = \frac{RT\rho_w}{M_w} \cdot \ln\varphi \tag{4.6}$$

where

R is the gas constant, with the value 8.314 J/(mol·K);
T is the temperature [K];
ρ_w is the density of water [kg/m^3];
M_w is the molar weight of water, with the value 0.018 kg/mol.

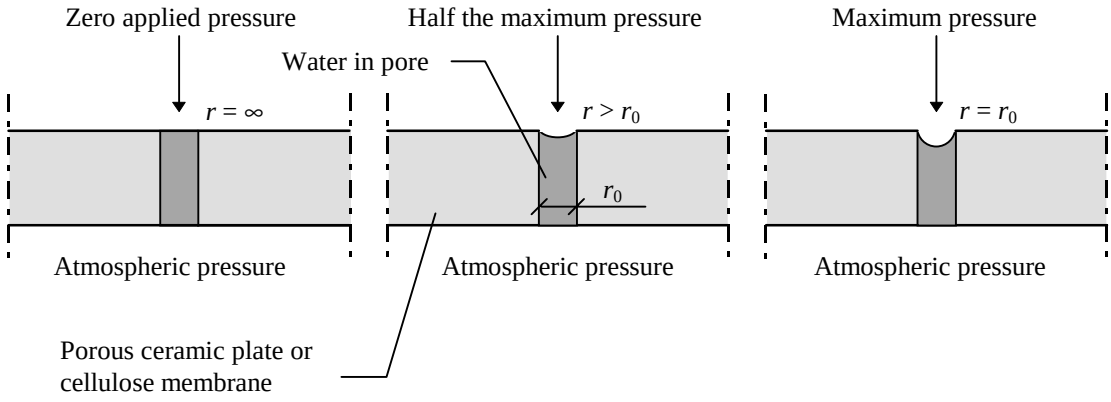

Figure 4.2 The function of the ceramic plate/cellulose membrane. A pressure difference is applied over the ceramic plate/cellulose membrane. The pores, as they are saturated with water, allow water but not air to pass through them. The maximum applied pressure that the ceramic plate/cellulose membrane can stand, before letting air pass through the pores, is determined by the radius of the pores, r_0.

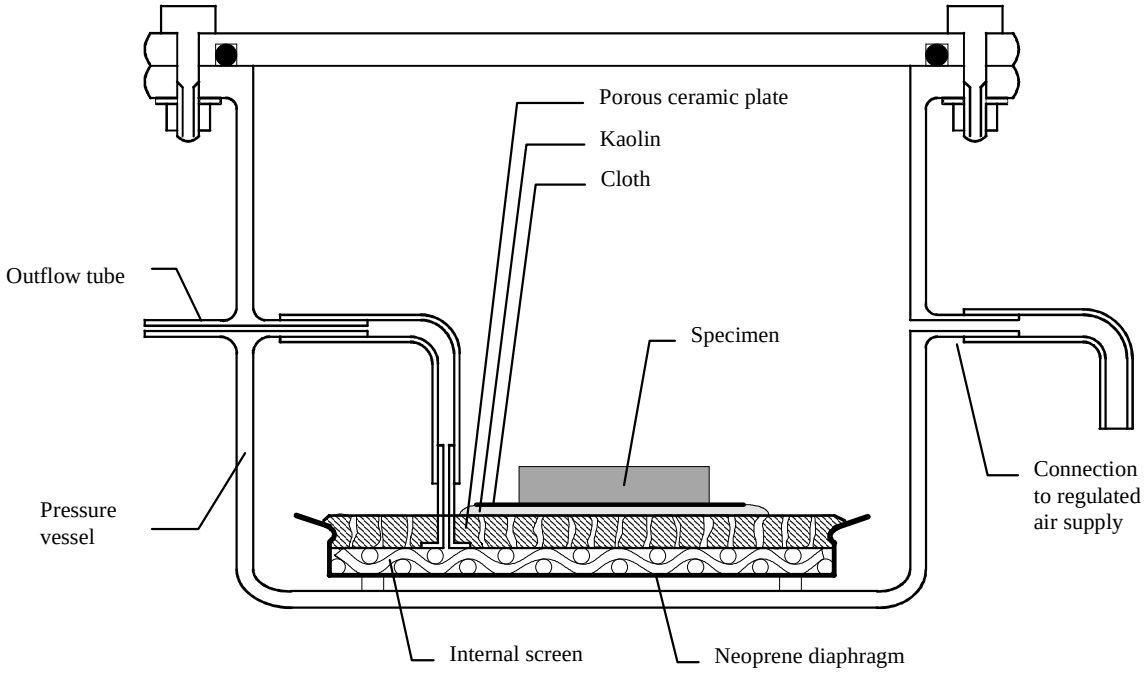

Figure 4.3 A sketch of a pressure plate extractor mounted in a pressure vessel. Excess water in the specimen is by overpressure forced out of the specimen through the cloth, kaolin clay, ceramic plate and out of the vessel. The internal screen prevents the neoprene diaphragm to clog the underside of the ceramic plate when pressure is applied. The connection between the internal screen and the outside of the vessel (the outflow tube) produces atmospheric pressure underneath the ceramic plate. The applied overpressure is regulated by a high quality manifold pressure regulator.

4.2.5 Rapid conditioning

If the two methods of evaluating the moisture diffusivity from the relation *A(w)* presented in Chapter 5 should be more extensively used, a more rapid method of conditioning the specimens must be used. Therefore a complementary rapid method of conditioning the specimens was tested.

The dry weight of the specimens was obtained by drying the specimens for 7 days at 105°C. Afterwards, the specimens were cooled in an exsiccator, using silica gel. The specimens were then weighed on a balance with a resolution of 1 mg. The specimens were placed in a plastic tray with de-ionized water. They were allowed to suck water until the desired initial moisture content was attained. To prevent moisture exchange with the surroundings, the specimens were wrapped in plastic. Thereafter the specimens were stored in the laboratory climate for 14 days before a capillary water uptake test was performed.

One cannot preclude the possibility that this conditioning creates moisture gradients in the specimen. The part closest to the water table is desorbed after water uptake is terminated; and the part that is further away from the water table absorbs water due to redistribution. However, the type of stone used seems to have a low moisture hysteresis. Therefore, the gradient might be rather limited.

4.2.6 Capillary water uptake test

In order to prevent evaporation from the sides and to create one dimensional flow, the sides of the specimens were sealed. In order to find a suitable sealant a pre-study was carried out with specimens sealed with beeswax, epoxy and a heavy aluminum tape. This study did not show any significant difference between the function of the beeswax and the aluminum tape. The epoxy did, however, somewhat penetrate the stone. The aluminum tape was finally chosen as sealant since the tape is easier to apply. It is also easier to remove without damaging the specimen.

When no change of weight could be observed for the specimen conditioned in climate boxes, the conditioning was considered as terminated and a nozzle was mounted onto the specimen. The nozzle was attached to the specimens with silicone, see Figure 4.4. The mounting took place in climate rooms with relative humidity and temperature similar to those in the climate boxes. In that way the specimens were disturbed as little as possible. After mounting the nozzles, the specimens were once again placed into the climate boxes for the silicone to cure. The capillary suction test took place the next day. Specimens conditioned in pressure extractors had their nozzles mounted before they were conditioned. The same applies to the specimens conditioned by the rapid conditioning. The capillary suction test could then take place directly after the conditioning.

During the capillary water uptake test the specimen absorbed de-ionized water from a reservoir. The specimen was connected to the reservoir through the nozzle and a liquid supply system (see Figure 4.5). Both the nozzle and the supply system were made of glass. A balance recorded the loss of weight of the water reservoir. The result was transmitted on-line, to a PC. Data could be recorded at an interval of 2 seconds. In order to prevent evaporation from the water reservoir, the balance was placed in a small chamber with approximately 100% relative humidity. The capillary water uptake test started by evacuating the air through a valve on the nozzle. In that way, the entire specimen end was

wetted. The nozzle was designed in such a way that the whole specimen surface was wetted within a few seconds. During the test the specimen was positioned horizontally.

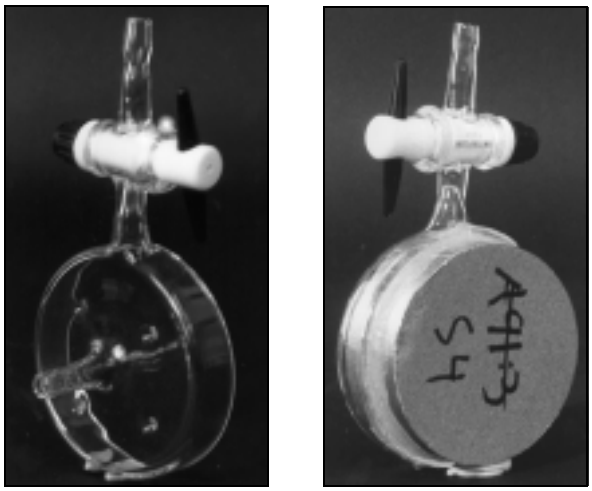

Figure 4.4 Nozzle without a specimen mounted (left) and with a specimen mounted (right). The specimen is sealed with aluminium tape and attached to the nozzle with silicone. On the top of the nozzle there is a valve, used to start the capillary suction test by evacuating air and wetting the specimen.

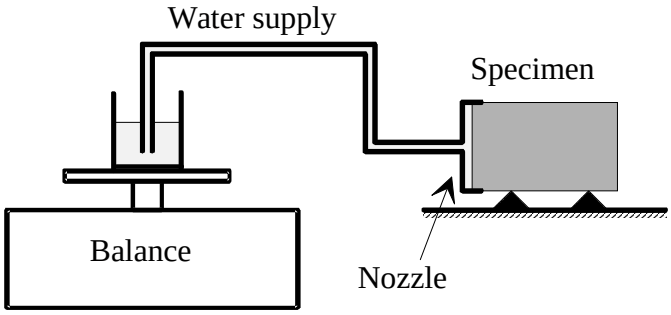

Figure 4.5 Schematic presentation of the laboratory set up. To prevent evaporation from the water reservoir, the balance is placed in a small chamber with approximately 100% relative humidity

4.2.7 Determination of density and porosity

To be able to calculate the moisture content mass per volume, *w*, from the moisture content mass per mass, *u*, the specimen density had to be known (see Eq. 4.2). The density was calculated as the ratio of the dry weight to the specimen volume. This was determined according to Archimedes' principle; the specimen was vacuum-saturated with water and weighed in air and in water. The volume and density were calculated from:

$$V = \frac{m_{air} - m_w}{\rho_w} \tag{4.7}$$

$$\rho = \frac{m_0}{V} \tag{4.8}$$

where

V is the specimen volume [m^3];
m_{air} is the vacuum saturated specimen weight in air [kg];
ρ_w is the density of water [kg/m^3];
ρ is the density of the specimen [kg/m^3];
m_w is the vacuum saturated specimen weight in water [kg];
m_0 is the dry weight [kg].

The vacuum saturation was performed using a procedure described by Fagerlund (1977):

1. The specimens are dried at 105°C and weighed. Then the specimens are evacuated in dryness in a exsiccator for 3 hours at a residual pressure of ~1-2 Torr.
2. Tap water at room temperature is let into the exsiccator while the pump is still running so that the specimens are covered with water within one minute.
3. The pump is run for one hour with water in the exsiccator.
4. Ordinary atmospheric pressure is let into the exsiccator.
5. The specimens are stored in water until determination of volume.

The weighing in air and water also enables determination of the porosity, Φ [m^3/m^3], and the compact density, ρ_c:

$$\Phi = \frac{m_{air} - m_0}{\rho_w \cdot V} \tag{4.9}$$

$$\rho_c = \frac{\rho}{1 - \Phi} \tag{4.10}$$

The capillary porosity, Φ_c, and the moisture content at capillary saturation, w_{cap}, were evaluated from capillary water uptake tests. The tests were performed on specimens dried at 105°C. Capillary water saturation is defined as the moisture content when the capillary water uptake comes to an almost complete halt. The capillary porosity is defined as the water filled porosity at the same time (see Figure 4.6). The moisture content continues to increase even after the rapid capillary suction has stopped. This process depends on air (in pores that are non active during capillary suction) dissolving in the water. This process is however, very slow.

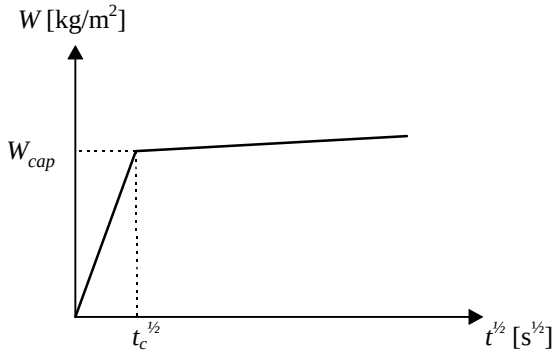

Figure 4.6 Capillary water uptake test used for determination of capillary water saturation and capillary porosity. The first quick water uptake comes to an end when the capillary transport stops. The moisture content continues to increase as a consequence of the air in non active pores dissolving in the water. This process is however, very slow.

4.3 Results

4.3.1 Capillary water uptake

The sorption coefficient, A [kg/(m^2·s^{½})] is defined by:

$$W = A\sqrt{t} \tag{4.11}$$

where

$W(t)$ is the amount of absorbed water [kg/m^2].

The sorption coefficient was measured by letting a pre-conditioned specimen suck water and automatically, on line, measure the amount of absorbed water. The amount of absorbed water per square meter was plotted as a function of the square root of time (see Figure 4.7).

The non linear shape of the curve in the first few seconds is probably caused by the gradual wetting process of the specimen surface. The decreasing slope at the end of the curve is caused by a gradually proceeding capillary saturation of the specimen. The slope of the linear part of the function gives the sorption coefficient, $A(w_{in})$ (see Figure 4.8).

Figure 4.9 shows sorption coefficients as a function of the initial water content. Each dot corresponds to one capillary water uptake test. The specimens were conditioned in the hygroscopic range in climate boxes, and in the superhygroscopic range by a pressure plate extractor (for pressures up to 15 bar) and a pressure membrane extractor (for pressures up to 100 bar), see sections 4.2.3 and 4.2.4.

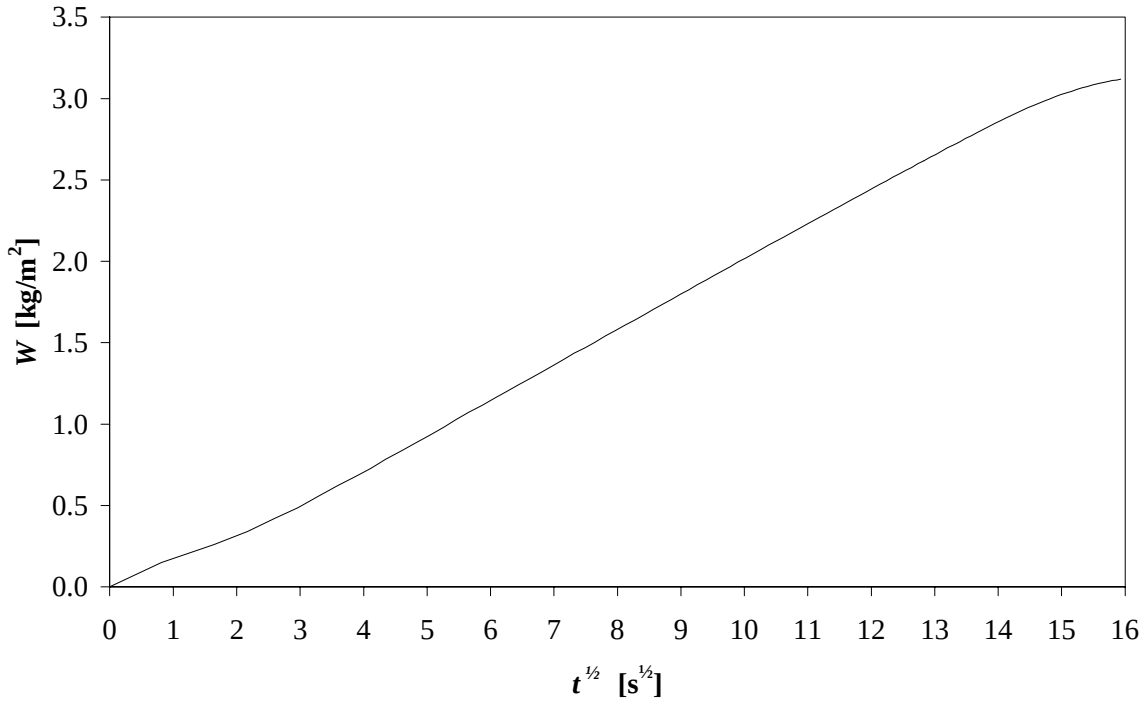

Figure 4.7 The amount of absorbed water per square meter W, is drawn as a function of the square root of time.

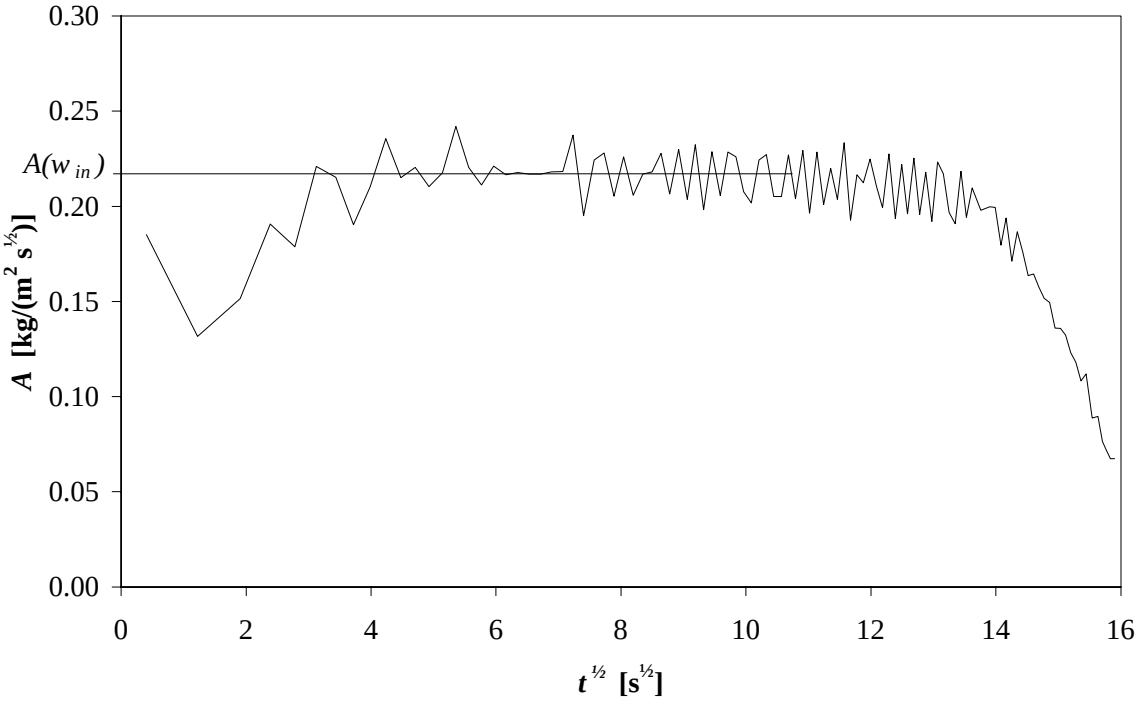

Figure 4.8 The slope of the curve in Figure 4.7; the sorption coefficient A, is ~0.22 kg/(m²·s½).

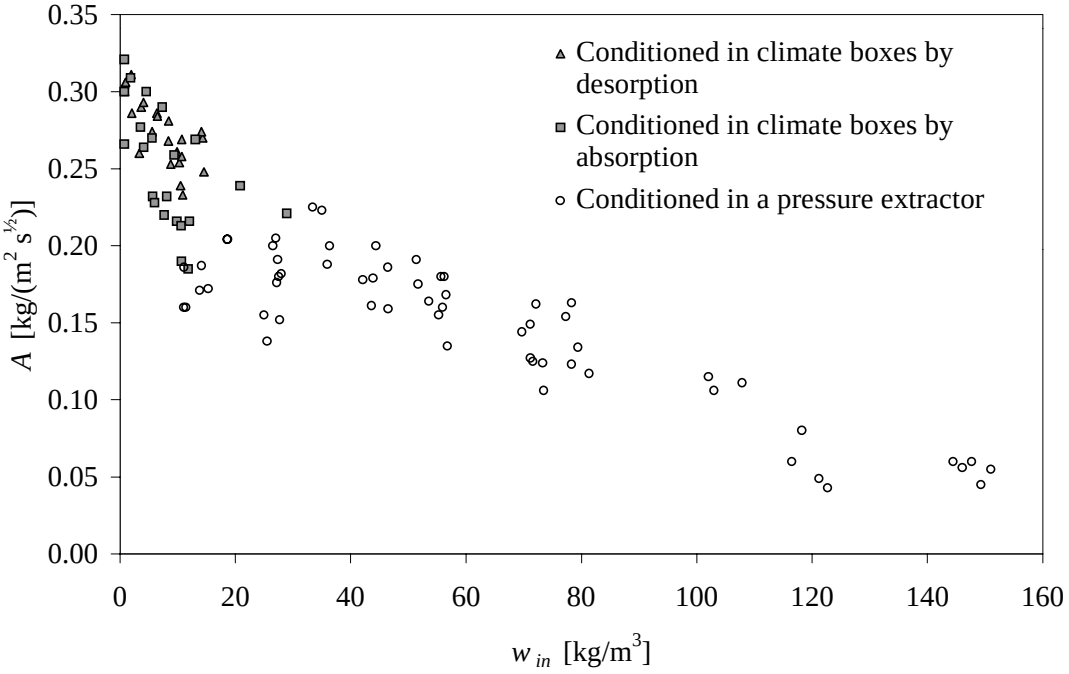

Figure 4.9 The sorption coefficient A, as a function of the initial water content expressed as mass by volume, w_{in}. Each dot represents one capillary water uptake test. The capillary saturation, w_{cap}, is approximately 160 kg/m³, see section 4.3.2.

As shown in Figure 4.9, the sorption coefficients vary strongly in the interval $0 \le w_{in} \le 20$ kg/m^3, which correspond to the hygroscopic range. One possible explanation of this variation is errors in the measuring procedure. However, this is unlikely; the same measuring procedure was used to determine the sorption coefficients in the entire interval $0 \le w_{in} \le w_{cap}$ (w_{cap} is defined as the water content when the rapid capillary water uptake comes to an end). Another explanation is that water is blocking critical passages in the pore system when the water content $w_{in} = 20$ kg/m^3 is reached. The water is then forced to do detours and the capillary water transport decreases.

Other possible explanations of the relation between the sorption coefficient and initial water content are obtained by an analysis of the mechanisms behind capillary transport and the variables describing capillary transport in a tube.

The water penetration coefficient, B [m/s^{½}], is defined by the following relation:

$$x = B\sqrt{t} \tag{4.12}$$

where

- x is the penetration depth of the water front during sorption from a water surface [m];
- t is the time [s].

The resistance against water penetration that a given material has, is called the water penetration resistance, M [s/m^2] and it is defined by:

$$t = M \cdot x^2 \tag{4.13}$$

where

$$M = \frac{1}{B^2} \tag{4.14}$$

According to a theoretical treatment of the movement in a cylindrical tube, the water penetration resistance in a horizontal tube is described by:

$$M = \frac{2\eta}{r_0 \sigma \cos\theta} \tag{4.15}$$

where

- η is the dynamic viscosity [Pa·s], for water it is 0.0018 Pa·s at 0°C and 0.0010 Pa·s at +20°C;
- r_0 is the tube radius [m];
- σ is the surface tension [N/m] (see Figure 4.10);
- θ is the contact angle (see Figure 4.10).

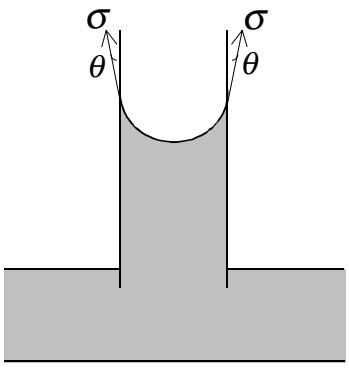

Figure 4.10 Capillary suction in a cylindrical tube with the surface tension, σ and the contact angle, θ.

In a porous material the pores are irregular. The water penetration resistance is therefore larger than in a tube and

cannot be described with Eq. 4.15. However, the equation shows the quantities that are influencing the water resistance coefficient in a porous material.

The sorption coefficient for a porous material can be calculated by:

$$A = \frac{\rho_w \Phi_a}{\sqrt{M}} \tag{4.16}$$

where

ρ_w is the density of water [kg/m^3];
Φ_a is the active porosity available for capillary transport [m^3/m^3].

Eq. 4.17 is obtained when Eq. 4.15 is combined with Eq. 4.16. Eq. 4.17 describes the quantities that influence the capillary transport and the sorption coefficient in a porous material. The equation, however, does not give any information about the magnitude of the sorption coefficient.

$$A \propto \rho_w \Phi_a \sqrt{\frac{r_0 \sigma \cos\theta}{2\eta}} \tag{4.17}$$

Eq. 4.17 shows that the sorption coefficient increases with (i) increasing porosity that is available for capillary transport, (ii) increasing pore radius, and (iii) increasing surface tension. The sorption coefficient decreases with increasing contact angle and increasing viscosity. As shown in Figure 4.9, the sorption coefficient also decreases when the initial water content increases. Most likely, this is due to the fact that the active porosity available for capillary transport decreases with increasing initial water content:

$$\Phi_a = \frac{w_{cap} - w_{in}}{\rho_w} \tag{4.18}$$

When the initial water content increases, the active pore radius decreases while the absorbed water layer on the pore walls gets thicker. Most likely, the decreasing radius has only a secondary effect on the sorption coefficient. However, the strongly varying sorption coefficient in the interval $0 \le w_{in} \le 20$ kg/m^3 can not be explained by any of these two described mechanisms.

Figure 4.11 shows the measured and the calculated relation between the active porosity available for capillary transport and the initial water content. The calculated results are based on Eq. 4.18. The active porosity is determined by:

$$\Phi_a = \frac{A\sqrt{t_c}}{\rho_w \ell} \tag{4.19}$$

where t_c [s] is the time until the specimen becomes capillary saturated and ℓ [m] is the specimen length in the direction of the water transport.

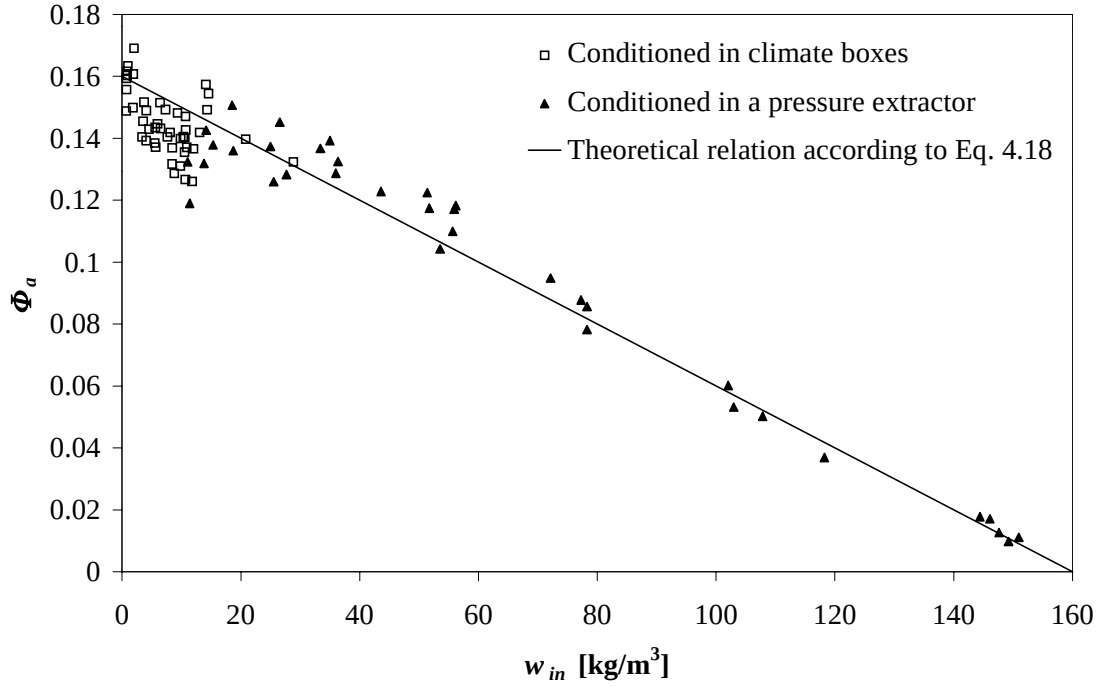

Figure 4.11 Active porosity available for capillary transport plotted against the initial water content. The line shows a theoretical relation between active porosity and initial water content, $A(w_{in})$, according to Eq. 4.18.

One probable explanation to the varying sorption coefficients in the interval $0 \leq w_{in} \leq 20$ kg/m^3 is that the surface tension increases at low initial water contents. According to Weast et al. (1989), the surface tension in a solution increases when the salt concentration increases. Since the sand stone is calcite bound, a certain amount of calcite is solved in the pore water. In the hygroscopic range, the specimens are conditioned in climate boxes. This process is relatively slow and the adsorbed water probably becomes saturated with calcite during the process. The conditioning process in the superhygroscopic range is done with pressure extractors and is quicker than the conditioning in the hygroscopic range. There will be less time for the calcite to solve in the pore water and the water will probably not be saturated with calcite. The concentration of solved calcite in the pore water is then higher at low initial water content (hygroscopic range). It will be an adsorbed water layer with high calcite concentration that will increase the surface tension when the capillary suction test starts. This layer will therefore increase the suction and the sorption coefficient.

Another possible explanation is that solved calcite has an influence on the contact angle. The contact angle may decrease when the calcite concentration increases. It is shown by Letey et al. (1962) that the contact angle varies strongly between water and sand, treated with NH_4OH of chaparral litter, water extract of chaparral litter and NH_4OH-starch solution, while the preparation has no effect on the contact angle between ethanol and sand.

In Figure 4.12 the sorption coefficient is plotted against the active porosity. In the Figure it is distinctly shown that specimens conditioned in climate boxes have higher sorption coefficients than specimens conditioned with pressure extractors at the same active porosity.

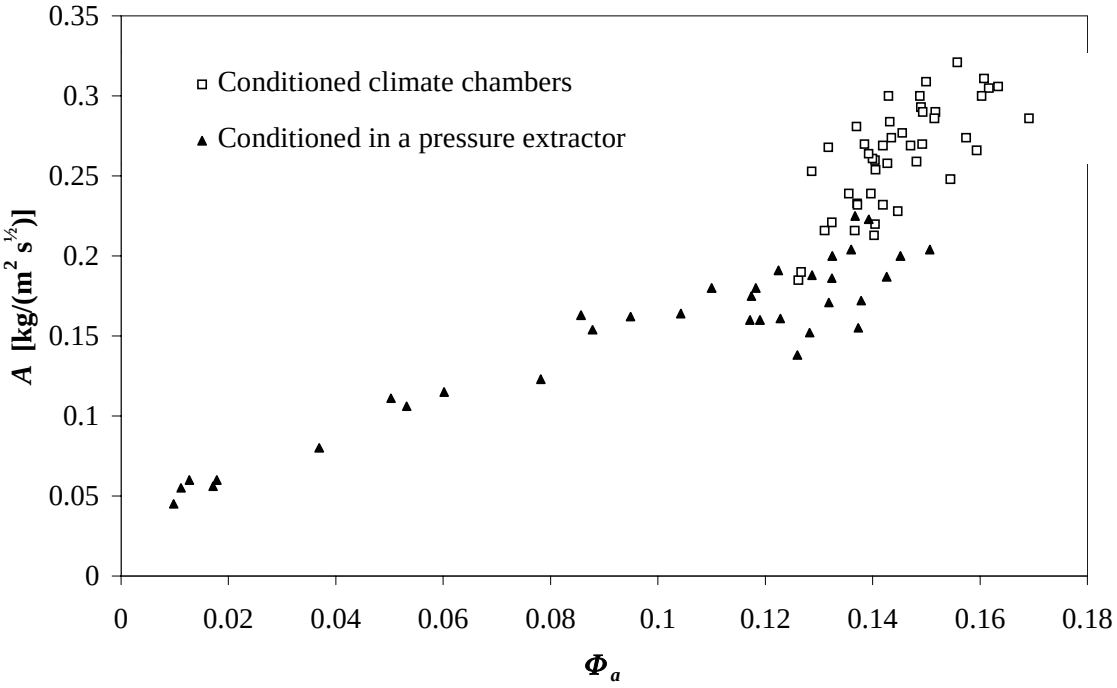

Figure 4.12 the sorption coefficient, A, plotted against active porosity, Φ_a.

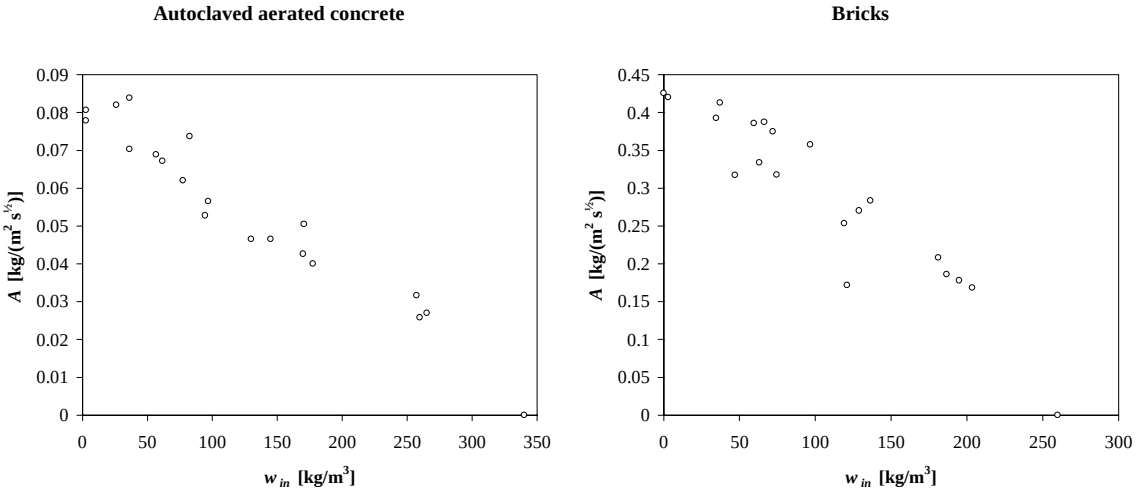

Figure 4.13 The sorption coefficient, A, as a function of initial water content, w_{in}. The capillary saturation, w_{cap}, is 340 kg/m^3 for the autoclaved aerated concrete and 260 kg/m^3 for the bricks (Schwarz 1972, Gösele et al. 1971).

Calcite is rather difficult to dissolve. Carbon dioxide-free water in equilibrium with calcite at 25°C dissolves 0.52 mg calcite per 100 g water and water saturated with carbon dioxide dissolves 38 mg calcite per 100 g water (Hägg 1984). Effectively, sandstone exposed to an acid environment will dissolve more calcite and possibly raise the sorption coefficients. The water used for the experiments was almost carbon dioxide-free.

In Schwarz (1972), and Gösele, et al. (1971) measurements were made on bricks and autoclaved aerated concrete to determine the relation between the sorption coefficient and the initial water content (see Figure 4.13). The specimens were conditioned by letting them absorb water until the desired initial moisture content was attained. Thereafter the specimens were sealed and stored at 50°C for several months (Schwarz 1972). These measurements do not indicate any significantly higher variations in the sorption coefficient at low initial water contents.

The reason for the rapid conditioning (section 4.2.5) is to find out whether the sorption coefficients measured on the specimens conditioned by this method differ from those measured on specimens conditioned in climate boxes or pressure extractors. It is reasonable to assume that there is no moisture gradient over the specimen body when climate boxes or pressure extractors are used. Figure 4.14 shows the sorption coefficients measured on specimens conditioned with the rapid method and sorption coefficients measured on specimens conditioned in climate boxes or pressure extractors. No significant difference exists between the different methods of conditioning. This indicates that there is no moisture gradient over the specimen volume after the rapid conditioning. Therefore, the method seems to be suitable for Uddvide sandstone. If this conditioning method is to be used on other materials, the sorption coefficient obtained must be compared with sorption coefficients obtained on specimens conditioned in climate boxes and pressure extractors for at least a couple of moisture levels. That would ensure there is no moisture gradient over the specimen volume.

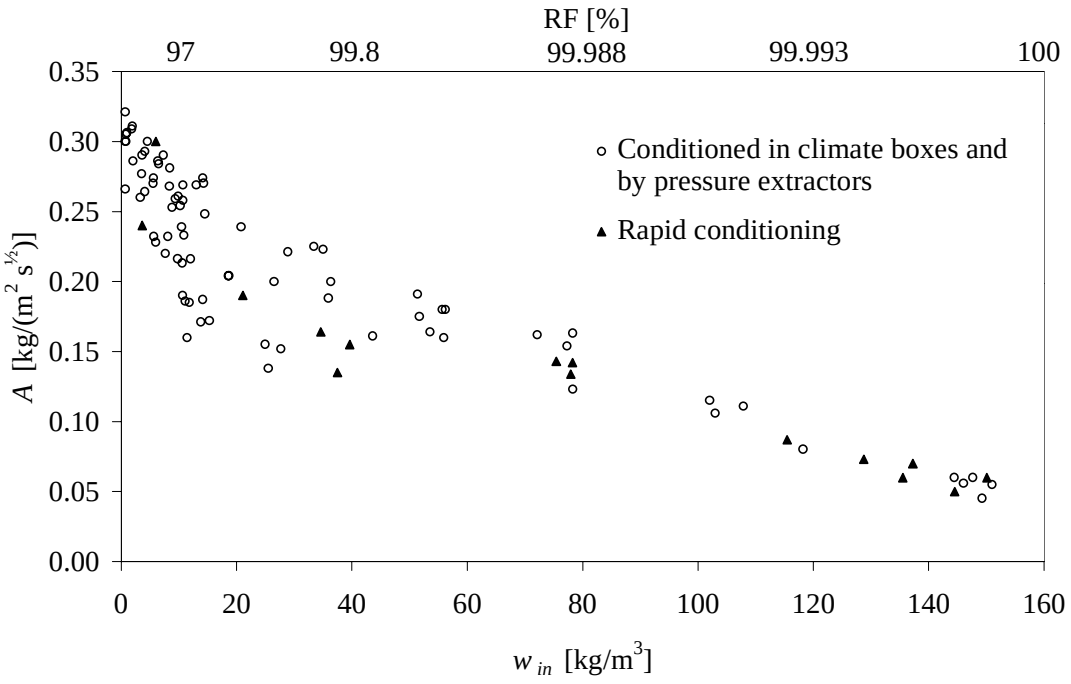

Figure 4.14 The sorption coefficients measured on specimens conditioned with the rapid method and sorption coefficients measured on specimens conditioned in climate boxes or pressure extractors.

4.3.2 Sorption isotherm, water retention curve , density and porosity

The density and the porosity were measured on every specimen used for capillary water uptake test, in total 48 specimens. The method used is described in section 4.2.7. The measured mean density of these specimens is 2059 kg/m^3 with a standard deviation of 6.5 kg/m^3. The mean porosity is 22.8% with a standard deviation of 0.25%. Figure 4.15 shows the distribution of measured density and porosity.

The capillary porosity, Φ_c, and the moisture content at capillary saturation, w_{cap}, were measured on 6 specimens. The method used is described in section 4.2.7. The results from the capillary water uptake test are shown in Figure 4.16. The capillary porosity and the moisture content at capillary saturation are evaluated from the amount of absorbed water when the first rapid capillary transport terminates. The magnitude of the capillary porosity and the moisture content at capillary saturation are 15.9% and 159.4 kg/m^3 respectively.

The moisture storage capacity was determined on the basis of the weight of the specimens conditioned for capillary water uptake test and on special specimens used only for this purpose (see section 4.2.2). In the hygroscopic range the specimens were conditioned in climate boxes both by absorption and desorption. In the superhygroscopic range, specimens were conditioned in pressure extractors, by desorption.

In the hygroscopic range, the normal way to show the moisture storage capacity is by a sorption isotherm, i.e. a plot of the moisture content expressed as mass by volume, w [kg/m^3] or mass by mass, u [kg/kg], as a function of the relative humidity, φ [-] (see the left graph in Figure 4.17). In the superhygroscopic range, several different ways are used to show the moisture storage capacity. The most natural choice is to use a water retention curve, i.e. a relation between the moisture content, w or u, and the capillary pressure, P_{cap} [Pa], in the water phase. This is due to the fact that relative humidity is an extremely insensitive factor in this range. Besides, the conditioning in the superhygroscopic range was executed by an applied air pressure in pressure extractors. The applied air pressure is equal to the capillary pressure, see Eq. 4.3 and Eq. 4.4.

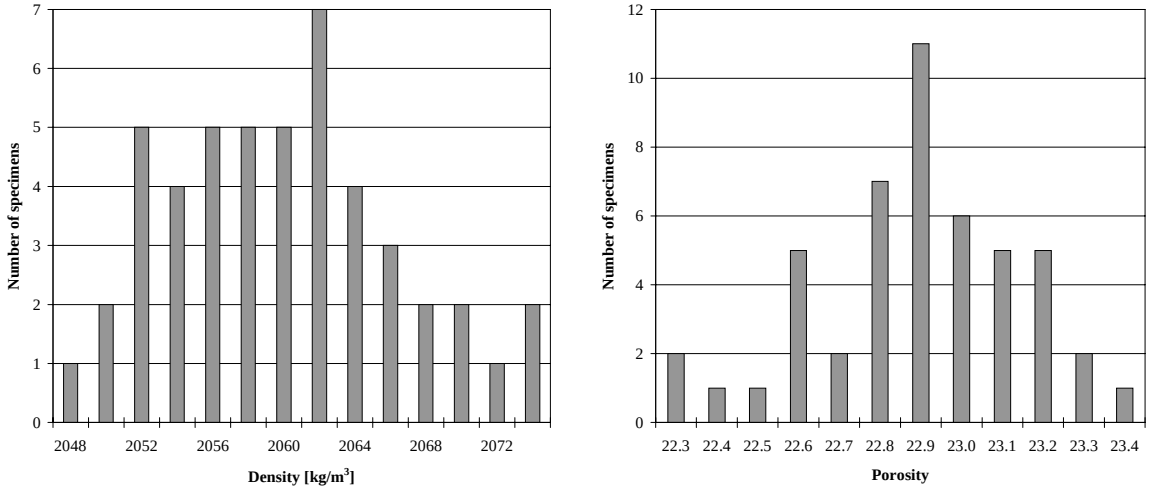

Figure 4.15 Distribution of measured density and porosity. The measured mean density is 2059 kg/m^3 with a standard deviation of 6.5 kg/m^3 and the mean porosity is 22.8% with a standard deviation of 0.25%.

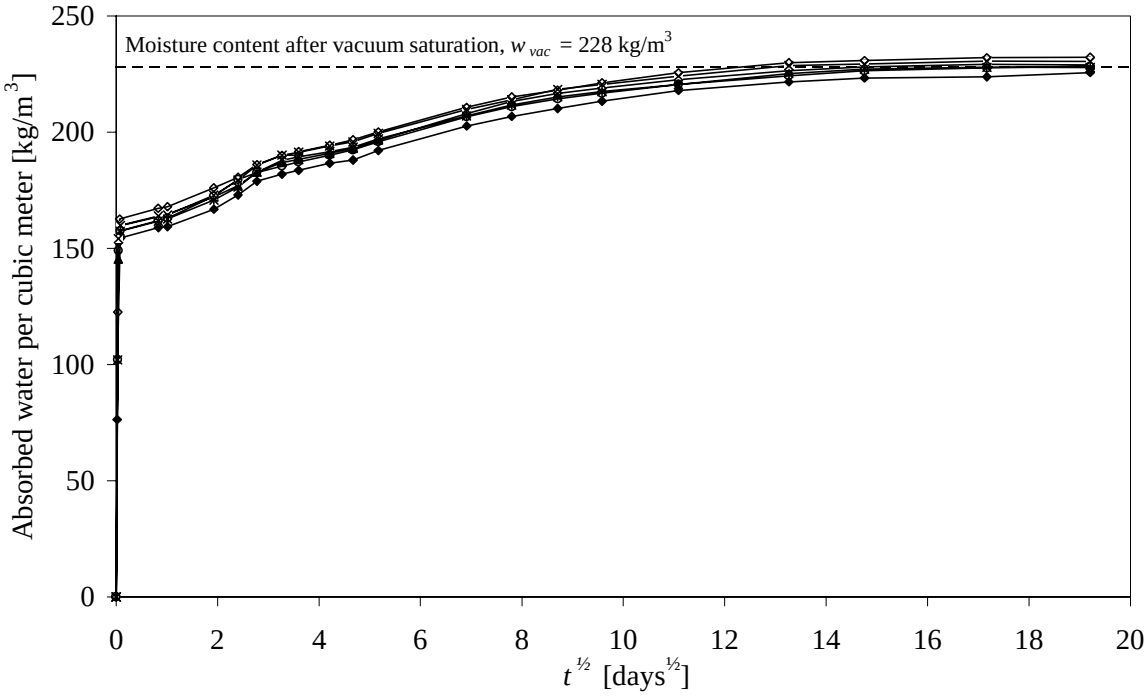

Figure 4.16 Determination of the capillary porosity and the water content at capillary saturation from a capillary water uptake test made on 6 specimens. Before testing them, the specimens were dried at 105°C. The figure also shows the slow water uptake taking place after that the capillary transport has stopped. The water content continue to increase until the same water content as after vacuum saturation is reached. This water content is obtained after approximately 230 days.

It is also possible to relate the pore pressure to the relative humidity. This is done with Kelvin's equation, Eq. 4.5. In the right graph in Figure 4.17 a water retention curve is shown both for the hygroscopic and the superhygroscopic range. The capillary pressures in the hygroscopic range are calculated from the relative humidity, using Kelvin's equation.

In the superhygroscopic range, the conditioning process starts by letting the specimen suck water for one day. The water content is then approximately 165 kg/m^3, see Figure 4.16. This value is exceeded for one specimen as shown in the right graph in Figure 4.17. This is due to the fact that the specimen continued to absorb water from the ceramic plate at the applied pressure. That is, the applied pressure was lower than the pressure at saturation. As shown in Figure 4.16, the sandstone continues to absorb water until all pores are filled with water and the moisture content is equal to the moisture content at vacuum saturation. This is due to a process other than capillarity.

It is also common to use the pore radius of a fictitious cylindrical pore instead of the pore pressure or relative humidity. The capillary pressure in a cylindrical pore can be described by:

$$P_{cap} = \frac{2\sigma \cos\theta}{r_0} \tag{4.20}$$

where

σ is the surface tension [N/m];
θ is the contact angle;
r_0 is the pore radius [m].

The contact angle is usually set to 0° which results in the following expression:

$$P_{cap} = \frac{2\sigma}{r_0} \tag{4.21}$$

The contact angle is probably not 0°. For example, it is 50° between a certain type of sand and water according to Letey et al. (1962). Besides, no pore in sandstone can be regarded as a cylinder. Therefore the error associated with using Eq. 4.21 is rather sizable. The contact angle between the sandstone used and water is unknown. However, according to Holmes (1965), sandstone differs from sand only in being coherent instead of loose. The contact angle between sandstone and water therefore, is probably the same as the contact angle between sand and water (i.e. almost 50°).

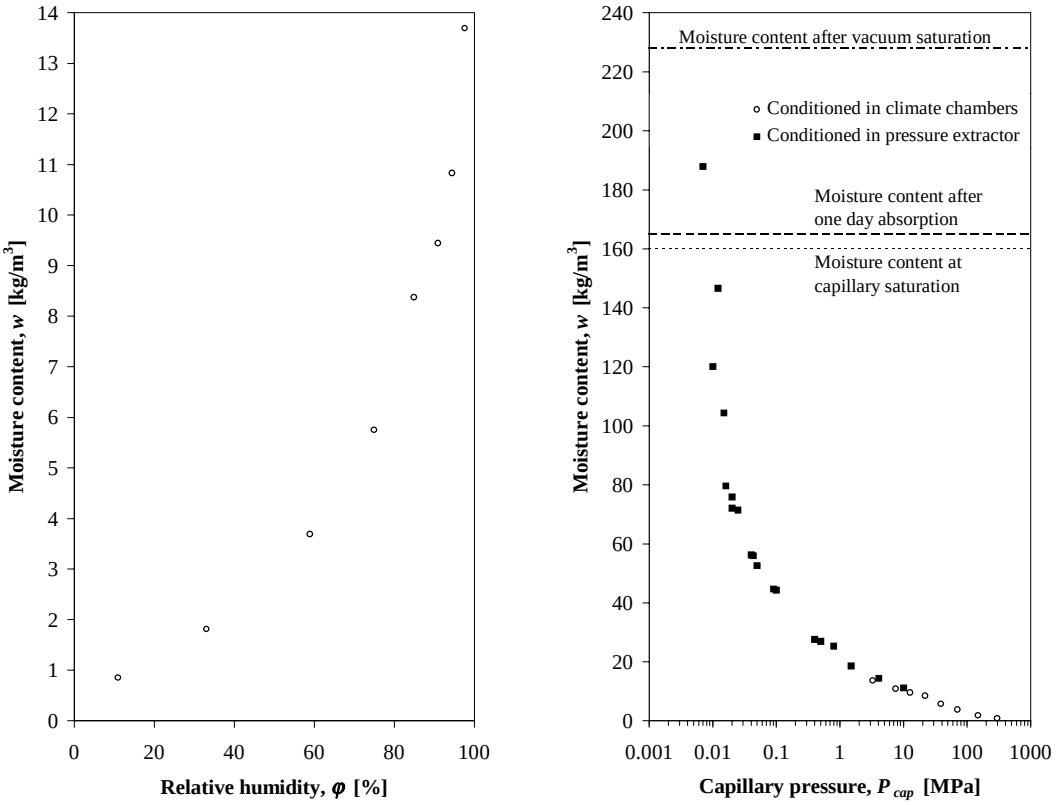

Figure 4.17 The moisture storage capacity of sandstone described by a sorption isotherm (left) and by a water retention curve (right). For the sorption isotherm, only measured values within the hygroscopic range are used. The water retention curve shows values from both the hygroscopic and the superhygroscopic range. The two methods of determining the storage capacity give overlapping results with no hysteresis.

5 Theoretical evaluation of the moisture diffusivity

5.1 Introduction

This chapter presents two methods of evaluating the moisture diffusivity, D_w [m^2/s], or the Kirchhoff flow potential, ψ [kg/(m·s)], at high moisture levels. The moisture diffusivity and the Kirchhoff flow potential are calculated from a series of sorption coefficients, A_1, A_2,..., A_N [kg/($m^2 \cdot s^{½}$)], corresponding to different initial water contents, $w_{in} = w_1$, w_2,..., w_N [kg/m^3] and the water content at capillary saturation, w_{cap}. The evaluation is done with both methods described and the results are compared. The input used is the result of capillary water uptake measurements performed with Uddvide Sandstone, presented in Chapter 4, and measurements performed with autoclaved aerated concrete and brick presented by Schwarz (1972) and Gösele et al. (1971).

If the mathematical formulation of capillary transport is correct, the moisture diffusivities are calculated exactly with the first evaluation method. From now on, this method is called Method 1. The method is based on the Boltzmann-transformation and was first presented in Claesson (1994). The second method is designated hereafter, as Method 2. It is based on an analytical solution of step response with two capacities, and is given in Arfvidsson (1994). Method 2 gives an approximate solution of the Kirchhoff flow potential.

The moisture diffusivity and the Kirchhoff flow potential measured in this study on Uddvide sandstone at high moisture levels are compered with the same parameters measured at low moisture levels by the cup method (Hedenblad 1996).

5.2 Methods of evaluation

5.2.1 General

The moisture diffusivity, D_w [m^2/s], and the Kirchhoff flow potential, ψ [kg/(m·s)], are calculated from a measured relation between the sorption coefficient, A [kg/($m^2 \cdot s^{½}$)], the initial water content, w_{in} [kg/m^3], and the water content at capillary saturation, w_{cap}. Both methods used imply that the moisture flux, g [kg/(m^2·s)], at steady state is described by Fick's law (here in one dimension):

$$g = -D_w \frac{\partial w}{\partial x} \tag{5.1}$$

The moisture balance equation, from which the moisture profiles at various times can be calculated, becomes:

$$\frac{\partial w}{\partial t} = \frac{\partial}{\partial x}\left(D_w \frac{\partial w}{\partial x} \right) \tag{5.2}$$

These two equations can also be described with the Kirchhoff flow potential, ψ, instead of the moisture diffusivity, D_w. The relation between Kirchhoff flow potential and moisture diffusivity are:

$$\psi = \psi_{ref} + \int_{w_{ref}}^{w} D_w dw \tag{5.3}$$

or

$$D_w = \frac{d\psi}{dw} \tag{5.4}$$

The reference value ψ_{ref} at $w = w_{ref}$ can be chosen arbitrarily. Here we choose $\psi_{ref} = 0$. The moisture flux with the Kirchhoff flow potential is described by:

$$g = -\frac{\partial \psi}{\partial x} \tag{5.5}$$

and the moisture balance equation becomes:

$$\frac{\partial w}{\partial t} = \frac{\partial^2 \psi}{\partial x^2} \tag{5.6}$$

or:

$$C_\psi \frac{\partial \psi}{\partial t} = \frac{\partial^2 \psi}{\partial x^2} \tag{5.7}$$

with the moisture capacity, C_ψ [s/m^2], defined by:

$$C_\psi = \frac{dw}{d\psi} = \frac{1}{D_w} \tag{5.8}$$

5.2.2 Method 1: Solution based on Boltzmann-transformation

If the mathematical formulation of capillary transport used above is correct, the moisture diffusivities are calculated exactly with this method. In the method which is based on Boltzmann-transformation the moisture diffusivity is calculated from a relation between the sorption coefficient, A, and the initial water content, w_{in}. This method of evaluation was first presented by Claesson (1994).

The Boltzmann-transformation gives an analytical solution for a step response in the semi-infinite volume. It is assumed that the moisture diffusivity is stepwise constant within a certain range of water contents:

$$D_w = \begin{cases} D_1 \colon w_{cap} > w > w_1 \\ D_2 \colon w_1 > w > w_2 \\ \vdots \\ D_N \colon w_{N-1} > w > w_N \end{cases} \tag{5.9}$$

N values of initial water contents, $w_{in} = w_1, w_2,..., w_N$, with the N corresponding values of sorption coefficients, $A = A_1, A_2,..., A_N$, are chosen from a measured relation $A(w_{in})$. With these values, and by knowing the water content at capillary saturation, w_{cap}, it is possible to determine the moisture diffusivity, $D_w = D_1, D_2,..., D_N$.

D_1 is calculated from the first interval w_1 to w_{cap}:

$$1. \quad w_{cap} - w_1 = \frac{\sqrt{\pi}\, A_1}{2\sqrt{D_1}} \tag{5.10}$$

D_2 is calculated in the second interval w_2 to w_1. Here $\eta_{2,1}$ is defined by step 1 and the moisture diffusivity, D_2, is defined by step 2:

$$1. \quad w_{cap} - w_1 = \frac{\sqrt{\pi}\, A_2}{2\sqrt{D_1}} \cdot \operatorname{erf}\left(\frac{\eta_{2,1}}{\sqrt{D_1}} \right) \tag{5.11a}$$

$$2. \quad w_1 - w_2 = \frac{\sqrt{\pi}\, A_2}{2\sqrt{D_2}} \cdot e^{\left(-\eta_{2,1}^2 \left(\frac{1}{D_1} - \frac{1}{D_2} \right) \right)} \cdot \operatorname{erfc}\left(\frac{\eta_{2,1}}{\sqrt{D_2}} \right) \tag{5.11b}$$

$\eta_{2,1}$ shows the penetration depth, x, of the level $w = w_1$ at the time, t (Claesson 1994, Crank 1975):

$$w = w_1 \text{ at } x = 2\eta_{2,1}\sqrt{t} \tag{5.12}$$

D_3 is calculated in three steps with A_3, w_3, D_1 and D_2. D_1 and D_2 are obtained from Eq. 5.10 and Eq. 5.11. This procedure is repeated until D_N is calculated in N steps. Step 1 to step N-1 gives $\eta_{N,1}$ to $\eta_{N,N-1}$ (each calculation gives new values $\eta_{N,i}$, these values do not show the penetration depth) and step N gives D_N:

$$1. \quad w_{cap} - w_1 = \frac{\sqrt{\pi}\, A_N}{2\sqrt{D_1}} \cdot \operatorname{erf}\left(\frac{\eta_{N,1}}{\sqrt{D_1}} \right) \tag{5.13a}$$

$$2. \quad w_1 - w_2 = \frac{\sqrt{\pi}\, A_N}{2\sqrt{D_2}} \cdot e^{\left(-\eta_{N,1}^2 \left(\frac{1}{D_1} - \frac{1}{D_2} \right) \right)} \cdot \left(\operatorname{erf}\left(\frac{\eta_{N,2}}{\sqrt{D_2}} \right) - \operatorname{erf}\left(\frac{\eta_{N,1}}{\sqrt{D_2}} \right) \right) \tag{5.13b}$$

$$\vdots$$

$$N\text{-}1. \quad w_{N-2} - w_{N-1} = \frac{\sqrt{\pi}\, A_N}{2\sqrt{D_{N-1}}} \cdot e^{\left(-\eta_{N,1}^2 \left(\frac{1}{D_1} - \frac{1}{D_2} \right) - \ldots - \eta_{N,N-2}^2 \left(\frac{1}{D_{N-2}} - \frac{1}{D_{N-1}} \right) \right)} \cdot \left(\operatorname{erf}\left(\frac{\eta_{N,N-1}}{\sqrt{D_{N-1}}} \right) - \operatorname{erf}\left(\frac{\eta_{N,N-2}}{\sqrt{D_{N-1}}} \right) \right) \tag{5.13N-1}$$

$$N. \quad w_{N-1} - w_N = \frac{\sqrt{\pi}\, A_N}{2\sqrt{D_N}} \cdot e^{\left(-\eta_{N,1}^2\left(\frac{1}{D_1} - \frac{1}{D_2}\right) - \ldots - \eta_{N,N-1}^2\left(\frac{1}{D_{N-1}} - \frac{1}{D_N}\right)\right)} \cdot \operatorname{erfc}\left(\frac{\eta_{N,N-1}}{\sqrt{D_N}}\right) \qquad (5.13N)$$

5.2.3 Numerical solution of Method 1

In order to be able to solve Eq. 5.10 to Eq. 5.13 a computer program has been developed by Arfvidsson and Janz (1994). The program uses the numerical solution presented in Claesson (1994), and Arfvidsson and Janz (1994). D_1 is calculated with Eq. 5.10:

$$D_1 = \frac{\pi A_1^2}{4\left(w_{cap} - w_1\right)^2} \qquad (5.14)$$

As shown in Eq. 5.11, D_2 is calculated in two steps. In the first step, $\eta_{2,1}$ is calculated by the inverse function of erf(x). Eq 5.11a gives:

$$\eta_{2,1} = \sqrt{D_1} \cdot \operatorname{erf}^{-1}\left(\frac{2\sqrt{D_1}\left(w_{cap} - w_1\right)}{\sqrt{\pi}\, A_2}\right) \qquad (5.15)$$

In the second step D_2, is calculated from Eq. 5.11b. The equation can be written so that all coefficients on the left-hand side of the equality are known and equal to K:

$$K = \frac{2\left(w_1 - w_2\right)}{A_2} \cdot e^{\frac{\eta_{2,1}^2}{D_1}} \cdot \eta_{2,1} = \sqrt{\pi} \cdot \frac{\eta_{2,1}}{\sqrt{D_2}} \cdot e^{\frac{\eta_{2,1}^2}{D_2}} \cdot \operatorname{erfc}\left(\frac{\eta_{2,1}}{\sqrt{D_2}}\right) \qquad (5.16)$$

In order to solve this equation, a function $\mathrm{e}_1(x)$ is introduced. By using this function in Eq. 5.16, D_2 can be solved:

$$K = \mathrm{e}_1\left(\frac{\eta_{2,1}}{\sqrt{D_2}}\right) \Rightarrow D_2 = \left(\frac{\eta_{2,1}}{\mathrm{e}_1^{-1}(K)}\right)^2 \qquad (5.17)$$

$\mathrm{e}_1^{-1}(y)$ is the inverse of the introduced function $\mathrm{e}_1(x)$. $\mathrm{e}_1(x)$ is defined by (see Figure 5.1):

$$\mathrm{e}_1(x) = \sqrt{\pi}\, x e^{x^2} \cdot \operatorname{erfc}(x) \qquad (5.18)$$

In the general case, with n = 2, 3,..., N, D_N is calculated with Eq. 5.13. In a way similar to in the case with two levels, Eq 5.13 is written so that all coefficients on the left-hand side of the equality are known and equal to K:

$$K = \frac{2\left(w_{N-1} - w_N\right)}{A_N} \cdot e^{\left(\eta_{N,1}^2\left(\frac{1}{D_1} - \frac{1}{D_2}\right) + \ldots + \eta_{N,N-1}^2 \cdot \frac{1}{D_{N-1}}\right)} \cdot \eta_{N,N-1} = \mathrm{e}_1\left(\frac{\eta_{N,N-1}}{\sqrt{D_N}}\right) \qquad (5.19)$$

Given the inverse function of $\mathrm{e}_1(x)$, D_N is calculated:

$$D_N = \left(\frac{\eta_{N,N-1}}{\mathrm{e}_1^{-1}(K)} \right)^2 \tag{5.20}$$

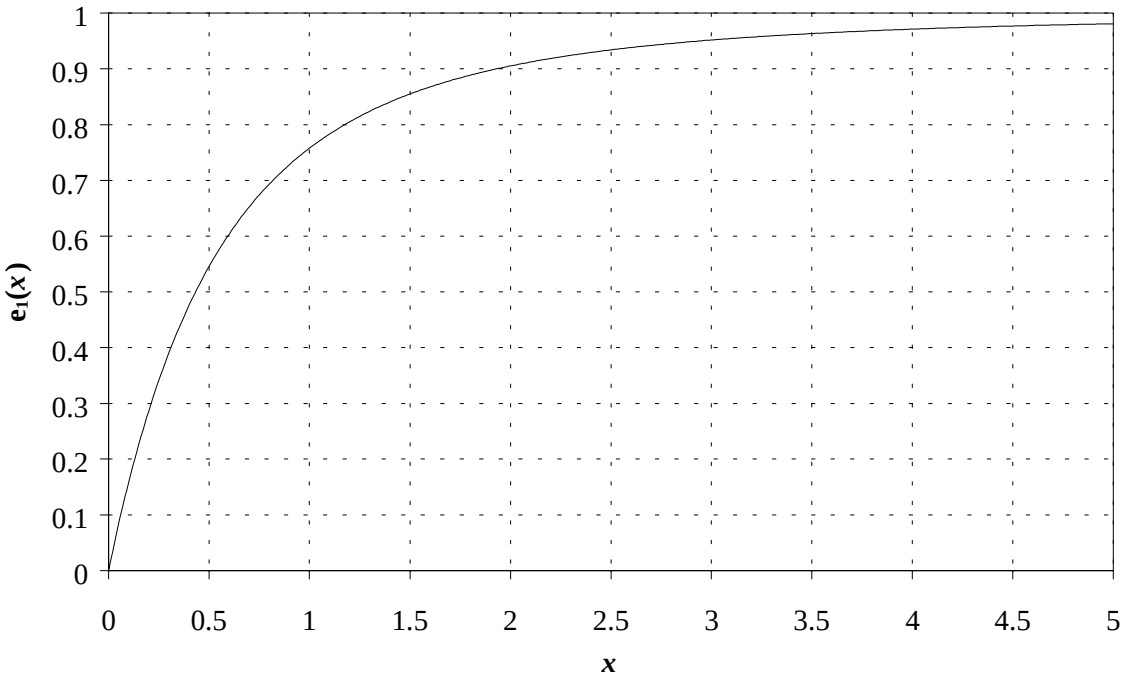

Figure 5.1 The function $e_1(x)$.

5.2.4 Method 2: Solution with two capacities

Method 2 is based on an analytical solution given by Arfvidsson (1994) of a step response with two capacities. This method gives an approximate solution of the Kirchhoff flow potential. In the special case, when the moisture capacity C_ψ is constant and $w(\psi)$ is linear (see Figure 5.2), it is possible, according to Arfvidsson (1994), to calculate the moisture capacity and the sorption coefficient, A, by:

$$C = C_1 = \frac{w_{cap} - w_{in}}{\psi_{cap} - \psi_{in}} \tag{5.21}$$

$$A_1 = \left(\psi_{cap} - \psi_{in} \right) \frac{2\sqrt{C_1}}{\sqrt{\pi}} = \frac{2}{\sqrt{\pi}} \sqrt{\left(w_{cap} - w_{in} \right) \left(\psi_{cap} - \psi_{in} \right)} \tag{5.22}$$

where

ψ_{cap} is the Kirchhoff flow potential at capillary saturation [kg/(m·s)]
ψ_{in} is the Kirchhoff flow potential at the water content w_{in} [kg/(m·s)]

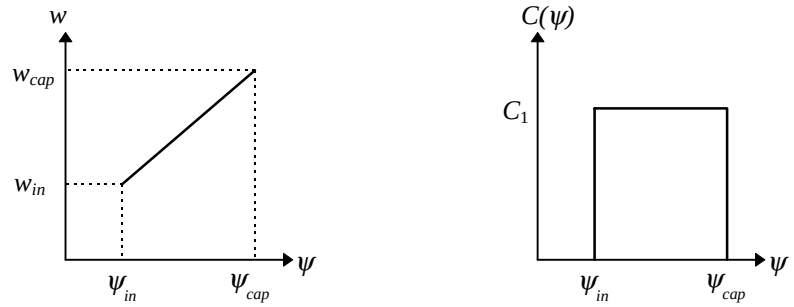

Figure 5.2 The moisture content, w(ψ), is linear and the moisture capacity C_ψ is constant.

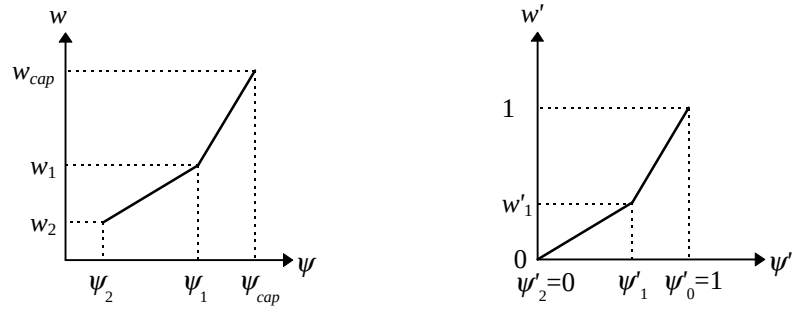

Figure 5.3 Linear moisture content, w(ψ) in the case with two capacities and the corresponding non-dimensional relation $w'(\psi')$.

In the general case Eq. 5.22 can be written with a non-dimensional sorption coefficient A_i' (Arfvidsson 1994):

$$A_i = \sqrt{\left(w_{cap} - w_{in}\right)\left(\psi_{cap} - \psi_{in}\right)} \cdot A_i' \tag{5.23}$$

For the special case with two moisture capacities (see Figure 5.3) and with $A_i = A_2$, Eq. 5.22 can be written as:

$$A_2 = \sqrt{\left(w_{cap} - w_2\right)\left(\psi_{cap} - \psi_2\right)} \cdot A_2'(\psi_1',\ w_1') \tag{5.24}$$

where

$$\psi_1' = \frac{\psi_{cap} - \psi_1}{\psi_{cap} - \psi_2} \tag{5.25}$$

and

$$w_1' = \frac{w_{cap} - w_1}{w_{cap} - w_2} \tag{5.26}$$

As in Arfvidsson (1994), A_2' can be written approximately as :

$$A_2' = \frac{2}{\sqrt{\pi}} + \left(\sqrt{2} - \frac{2}{\sqrt{\pi}}\right)\left(\psi_1' - w_1'\right) \qquad \text{when} \quad w_1' < 0.5 \text{ and } \psi_1' > 0.5 \tag{5.27}$$

Eq. 5.25 and Eq. 5.26 inserted to Eq. 5.27 gives:

$$A_2' = \frac{2}{\sqrt{\pi}} + \left(\sqrt{2} - \frac{2}{\sqrt{\pi}}\right)\left(\frac{\psi_{cap} - \psi_1}{\psi_{cap} - \psi_2} - \frac{w_{cap} - w_1}{w_{cap} - w_2}\right) \tag{5.28}$$

Eq. 5.24 can, in combination with Eq. 5.28, be written as:

$$a\left(\psi_{cap} - \psi_2\right)^2 + b\left(\psi_{cap} - \psi_2\right) + c = 0 \tag{5.29}$$

with the solution:

$$\left(\psi_{cap} - \psi_2\right) = -\frac{b}{2a} \pm \sqrt{\left(\frac{b}{2a}\right)^2 - \frac{c}{a}} \tag{5.30a}$$

a, *b* and c are known:

$$a = \left(\frac{4}{\pi} - \frac{4}{\sqrt{\pi}}\left(\sqrt{2} - \frac{2}{\sqrt{\pi}}\right)\cdot\frac{w_{cap} - w_1}{w_{cap} - w_2} + \left(\sqrt{2} - \frac{2}{\sqrt{\pi}}\right)^2 \cdot \left(\frac{w_{cap} - w_1}{w_{cap} - w_2}\right)^2\right)\cdot\left(w_{cap} - w_2\right) \tag{5.30b}$$

$$b = \left(\psi_{cap} - \psi_1\right)\left(\frac{4}{\sqrt{\pi}}\left(w_{cap} - w_2\right)\left(\sqrt{2} - \frac{2}{\sqrt{\pi}}\right) - 2\left(w_{cap} - w_1\right)\left(\sqrt{2} - \frac{2}{\sqrt{\pi}}\right)^2\right) - A_2^2 \tag{5.30c}$$

$$c = \left(\sqrt{2} - \frac{2}{\sqrt{\pi}}\right)^2 \cdot \left(w_{cap} - w_2\right)\left(\psi_{cap} - \psi_1\right)^2 \tag{5.30d}$$

In order to solve the above described equations, the following method of calculation is used:

1: ψ_{cap} - ψ_1:

ψ_{cap} - ψ_1 is calculated exactly by Eq. 5.22 with $w_{in} = w_1$ and $\psi_{in} = \psi_1$ (compare this equation with Eq 5.14; $\Delta\psi = D \cdot \Delta w$):

$$\left(\psi_{cap} - \psi_1\right) = \frac{A_1^2\,\pi}{4\left(w_{cap} - w_1\right)} \tag{5.31}$$

2: ψ_{cap} - ψ_2:

ψ_{cap} - ψ_2 is calculated with Eq. 5.30.

3: ψ_{cap} - ψ_i:

In order to be able to calculate the difference ψ_{cap} - ψ_i where i = 3,..., N, $\psi(w)$ is approximated linearly for $w_{cap} > w > w_{i-1}$. In that way ψ_{cap} - ψ_i can be calculated in the same way as in the special case with two capacities, i.e. with Eq. 5.30 with $w_2 = w_i$ and $A_2 = A_i$:

$$\left(\psi_{cap} - \psi_i\right) = -\frac{b}{2a} \pm \sqrt{\left(\frac{b}{2a}\right)^2 - \frac{c}{a}} \tag{5.32a}$$

$$a = \left(\frac{4}{\pi} - \frac{4}{\sqrt{\pi}}\left(\sqrt{2} - \frac{2}{\sqrt{\pi}}\right) \cdot \frac{w_{cap} - w_{i-1}}{w_{cap} - w_i} + \left(\sqrt{2} - \frac{2}{\sqrt{\pi}}\right)^2 \left(\frac{w_{cap} - w_{i-1}}{w_{cap} - w_i}\right)^2\right)\left(w_{cap} - w_i\right) \tag{5.32b}$$

$$b = \left(\psi_{cap} - \psi_{i-1}\right)\left(\frac{4}{\sqrt{\pi}}\left(w_{cap} - w_i\right)\left(\sqrt{2} - \frac{2}{\sqrt{\pi}}\right) - 2\left(w_{cap} - w_{i-1}\right)\left(\sqrt{2} - \frac{2}{\sqrt{\pi}}\right)^2\right) - A_i^2 \tag{5.32c}$$

$$c = \left(\sqrt{2} - \frac{2}{\sqrt{\pi}}\right)^2 \cdot \left(w_{cap} - w_i\right)\left(\psi_{cap} - \psi_{i-1}\right)^2 \tag{5.32d}$$

ψ' and w' becomes:

$$\psi'_{i-1} = \frac{\psi_{cap} - \psi_{i-1}}{\psi_{cap} - \psi_i} \tag{5.33}$$

$$w'_{i-1} = \frac{w_{cap} - w_{i-1}}{w_{cap} - w_i} \tag{5.34}$$

5.3 Results

5.3.1 Input data

The sorption coefficients obtained experimentally for Uddvide sandstone in Chapter 4 and the sorption coefficients of autoclaved aerated concrete and bricks presented by Schwarz (1972) and Gösele et al. (1971) are used as input to both of the methods.

In Figure 5.4 the experimental relation between the sorption coefficient and the initial water content, $A(w_{in})$, of Uddvide sandstone is shown. The experimental method used when measuring this relation is described in Chapter 4.

The relation between the sorption coefficient and the initial water content, $A(w_{in})$, of autoclaved aerated concrete and bricks is shown in Figure 5.5. This relation is reported by Schwarz (1972) and Gösele et al. (1971). The specimens were conditioned by letting them absorb water until the desired initial moisture content was attained. Thereafter, the specimens were sealed and stored at 50°C for several month before the test started (Schwarz 1972).

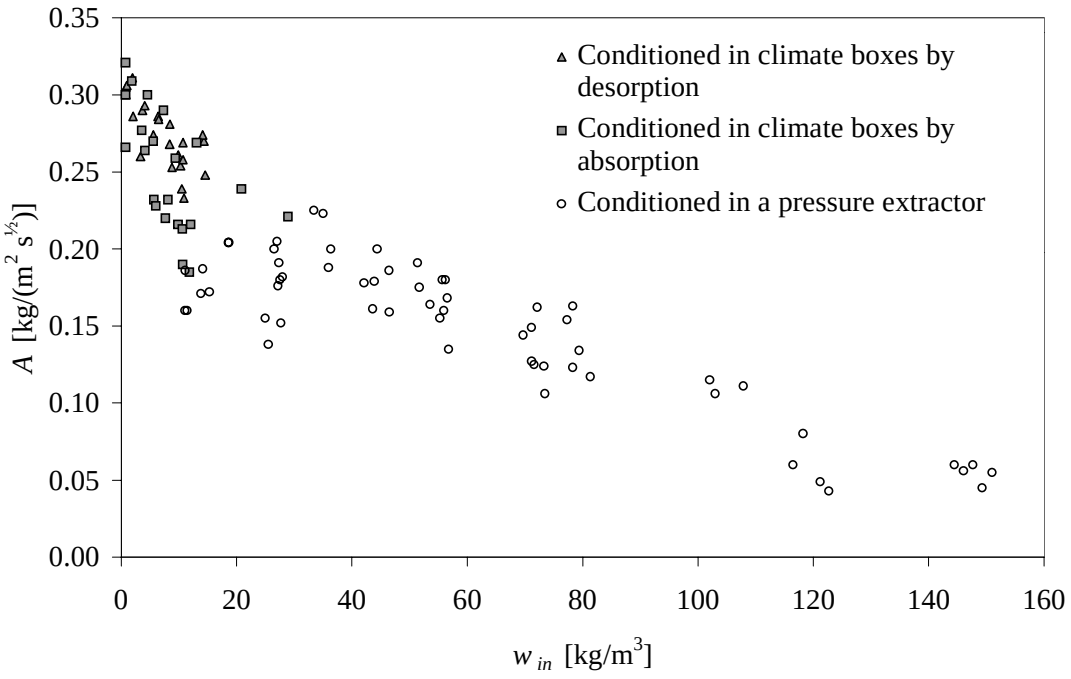

Figure 5.4 Experimentally determined sorption coefficient A, as a function of initial water content mass by volume, w_n for Uddvide sandstone. Each dot represents one capillary water uptake test. The capillary saturation, w_{cap}, is approximately 160 kg/m^3.

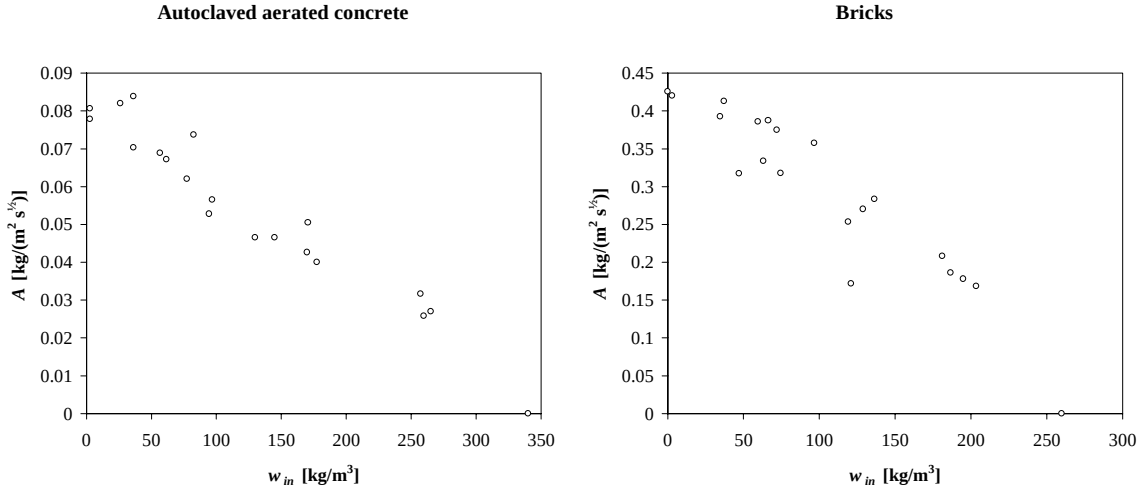

Figure 5.5 Experimentally determined sorption coefficient, A, as a function of initial water content, w_{in}. The capillary saturation, w_{cap}, is 340 kg/m^3 for the autoclaved aerated concrete and 260 kg/m^3 for the bricks (Schwarz 1972, Gösele et al. 1971).

5.3.2 Evaluation of the moisture diffusivity with Method 1

From the measured relation $A(w_{in})$ for Uddvide sandstone shown in Figure 5.4, N values of the initial water content $w_{in} = w_1, w_2,..., w_N$ together with the corresponding sorption coefficients $A = A_1, A_2,..., A_N$ are chosen. Using these values together with the moisture content at capillary saturation w_{cap} the moisture diffusivity $D(w_{in})$ is calculated. Different choices of the input values give different calculated moisture diffusivities. In Figure 5.6 and Appendix A the data used to calculate the moisture diffusivities of Uddvide sandstone are shown.

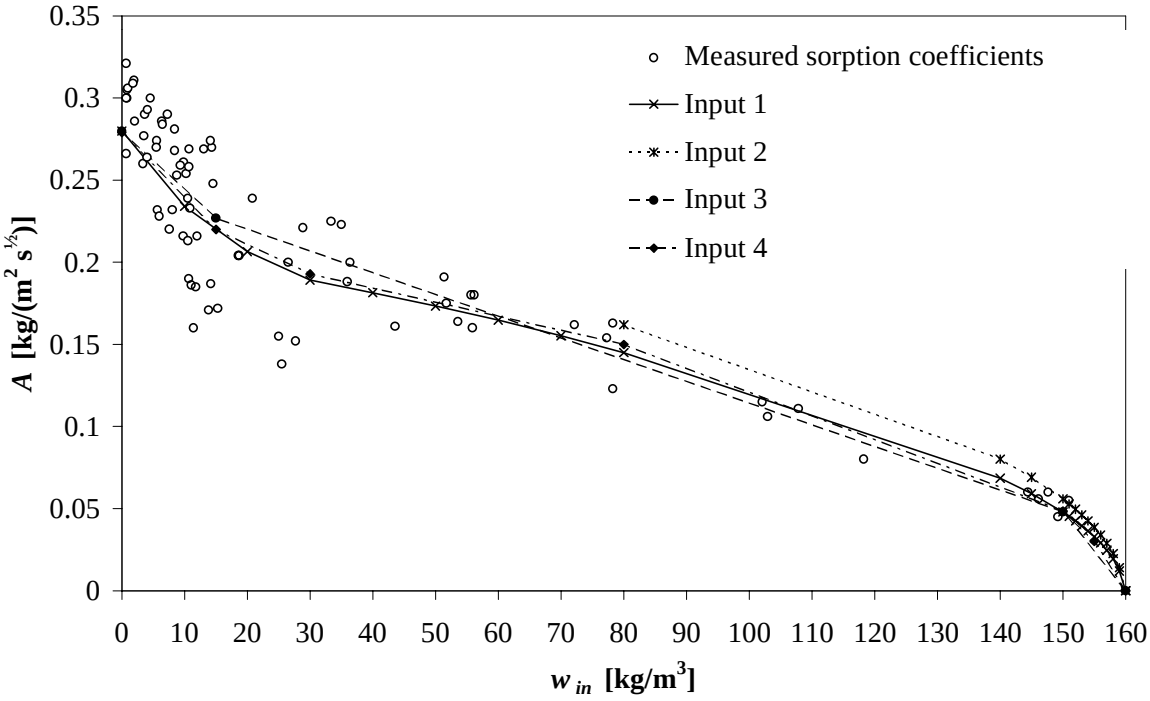

Figure 5.6 The input data used for calculation of moisture diffusivities of Uddvide sandstone. See also Appendix A.

When calculating the moisture diffusivity by Method 1, erf(x) in Eq. 5.15 and the function $e_1(x)$ used in Eq. 5.17 and Eq. 5.20 are inverted. These two inverses limit the possible choices of input values since $-1 < \text{erf}(x) < 1$ and $e_1(x) < 1$. Therefore, the conditions that must be fulfilled in Eq 5.15 are:

$$-1 < \left(\frac{2\sqrt{D_1} \cdot \left(w_{cap} - w_1 \right)}{\sqrt{\pi}\, A_2} \right) < 1 \tag{5.35}$$

Also for Eq. 5.17 and Eq. 5.20:

$$K = \frac{2\left(w_{N-1} - w_N \right)}{A_N} \cdot e^{\left(\eta_{N,1}^2 \left(\frac{1}{D_1} - \frac{1}{D_2} \right) + \ldots + \eta_{N,N-1}^2 \cdot \frac{1}{D_{N-1}} \right)} \cdot \eta_{N,N-1} < 1 \tag{5.36}$$

As shown in section 5.2.3, the calculation of the moisture diffusivity $D(w)$ starts at capillary saturation. Then, gradually lower initial water contents are used. This means that the first input value chosen, (w_1, A_1), will control the possible choice of the rest of the input values. For 'Input 2' in Figure 5.6 and Appendix A, the first input values chosen, w_1 and A_1, are 159 kg/m^3 and 0.014 kg/(m^2·s^{½}) respectively. Thereafter, the lowest possible values of A_2 to A_{13} are chosen. In spite of this, the $A(w)$ curve ends above the measured sorption coefficients, see Figure 5.6. For 'Input 1' in Figure 5.6 and Appendix A, all initial moisture contents chosen are equal to the moisture contents in 'Input 2'. The first sorption coefficient is however lowered from 0.014 kg/(m^2·s^{½}) to A_1 = 0.012 kg/(m^2·s^{½}). From w_{in} = 158 kg/m^3 to w_{in} = 140 kg/m^3 the lowest possible values of A(158) to A(140) are

chosen. Contrary to 'Input 2', in which $A_1 = 0.014$ kg/(m^2·s^{½}), 'Input 1', for which $A_1 = 0.012$ kg/(m^2·s^{½}), represents the measured sorption coefficients quite well. This shows the sensitivity that Eq. 5.35 and 5.36 entail and the importance of the choice of the first sorption coefficient $A(w_1)$.

The moisture diffusivity *D(w)* has also been calculated from two more possible choices of input values, 'Input 3' and 'Input 4'. These two have not as many input values as 'Input 1' and 'Input 2', see Figure 5.6 and Appendix A.

The results of all the calculations are presented in Figure 5.7. In comparison with results obtained from measurements with the cup-method (Hedenblad 1996), the calculated moisture diffusivities are unreasonably large when $w < 25$ kg/m^3.

Eq. 3.7 gives an approximate method for calculating the moisture diffusivity from one absorption test, for an initially dry specimen. This method was suggested by Künzel (1995) on basis of unknown theory. The result of Eq. 3.7 with $A = 0.28$ kg/(m^2·s^{½}) is shown in Figure 5.7.

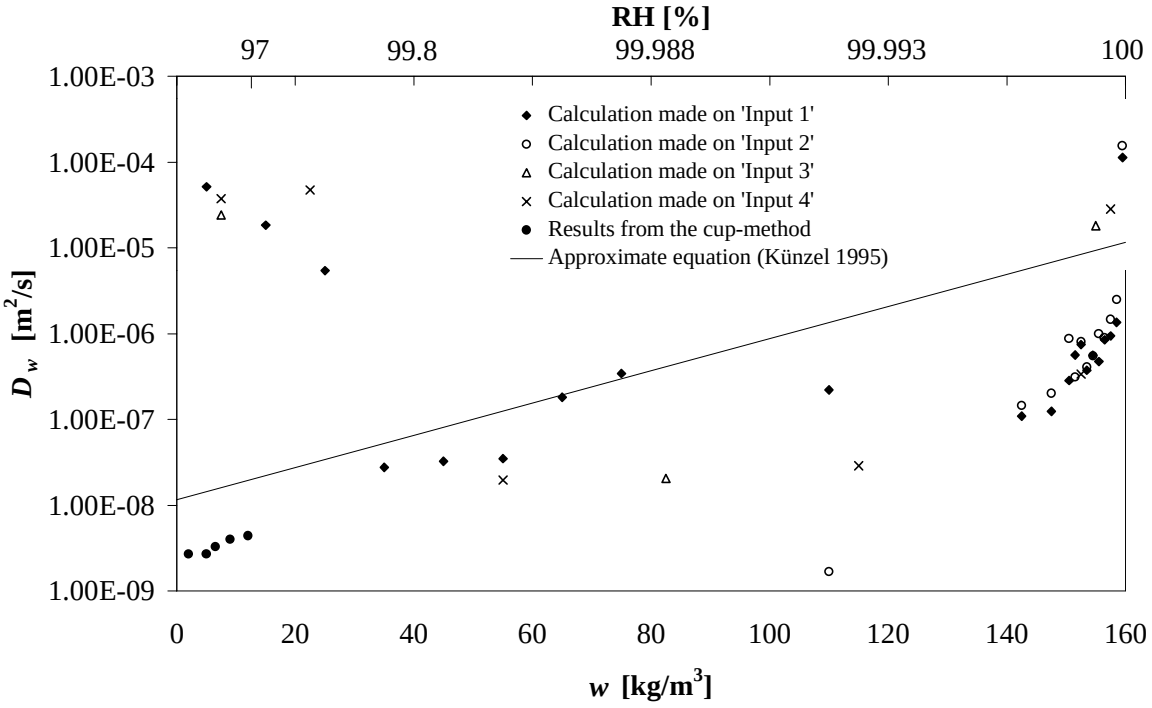

Figure 5.7 The moisture diffusivity obtained on Uddvide, D_w [m^2/s], calculated with 'Input 1' to 'Input 4', see Figure 5.6 and Appendix A. The input values in 'Input 2' are out of range. In comparison with results obtained from measurements with the cup-method (Hedenblad 1996), the calculated moisture diffusivities are unreasonably large when w *< 25 kg/m^3.*

From the relation *D(w)* obtained on Uddvide sandstone, the relation between the Kirchhoff flow potential and initial moisture content *ψ(w)* is calculated, see Figure 5.9. Eq. 5.3 shows the relation between the moisture diffusivity and the Kirchhoff flow potential:

$$\psi = \psi_{ref} + \int_{w_{ref}}^{w} D_w dw$$

i.e., ψ is the area under the function *D(w)*. The relation *ψ(w)* obtained by the cup-method is given by Hedenblad (1996). The following equations are used to calculate the Kirchhoff flow potential from the moisture diffusivity obtained with Method 1, and connect this flow potential with the flow potential obtained with the cup-method, see Figure 5.8:

$$\psi(w_N) = \left(w_N - w_{cup,\,max}\right) \cdot \frac{D_N + D_{cup,\,max}}{2} + \psi_{cup,\,max} \tag{5.37a}$$

$$\psi(w_{N-1}) = \left(w_{N-1} - w_N\right) \cdot D_N + \psi(w_N) \tag{5.37b}$$

$$\vdots$$

$$\psi(w_{cap}) = \left(w_{cap} - w_1\right) \cdot D_1 + \psi(w_1) \tag{5.37c}$$

where

$w_{cup,\,max}$ is the highest moisture content used with the cup-method [kg/m^3]
$D_{cup,\,max}$ is the moisture diffusivity obtained with the cup-method at $w_{cup,\,max}$ [m^2/s]
$\psi_{cup,\,max}$ is the Kirchhoff flow potential obtained with the cup-method at $w_{cup,\,max}$ [kg/(m·s)]

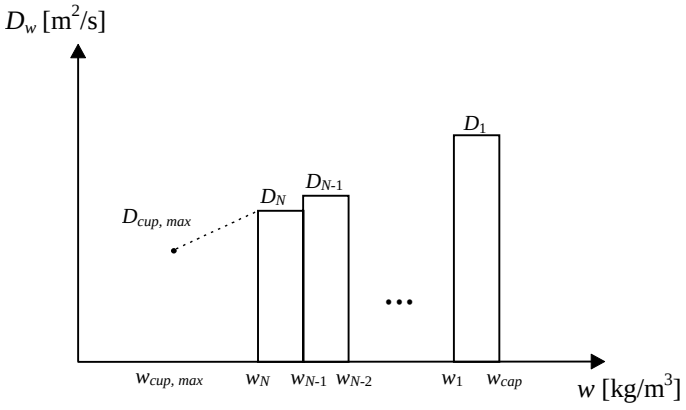

Figure 5.8 The principle used when calculating the ψ-values from the relation D(w) obtained with Method 1 and connecting this ψ(w) relation with the relation of ψ(w) given by the cup-method.

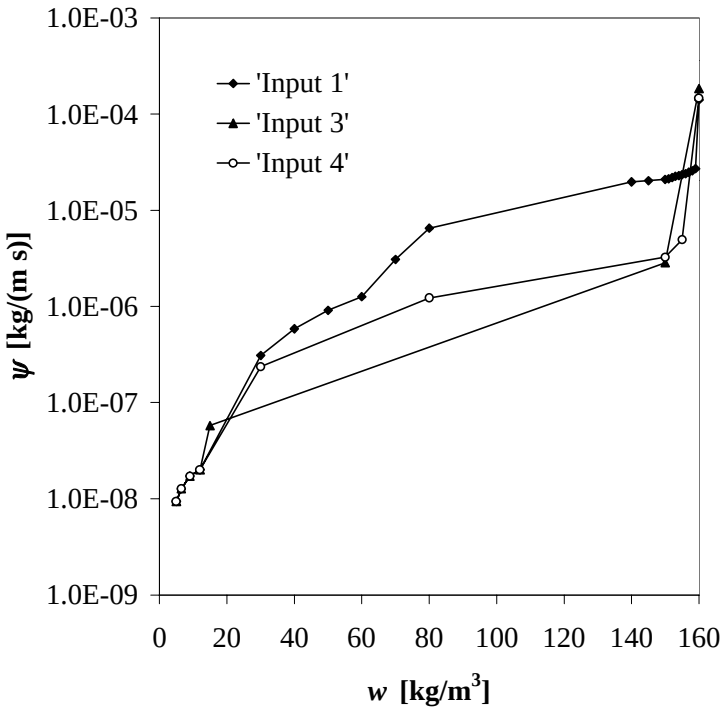

Figure 5.9 Results from the calculation with Method 1 and the cup-method (the first four ψ-values) of Kirchhoffs flow potential ψ(w) on Uddvide sandstone. The calculations are performed with 'Input 1', 'Input 3' and 'Input 4', see Figure 5.6 and Appendix A.

Moisture diffusivities of three different German sandstones, obtained from measurements of the moisture distribution with nuclear magnetic resonance (NMR), are reported by Krus (1995). The magnitude of the moisture diffusivities obtained with NMR on 'Rüthener Sandstein' is the same as that of the moisture diffusivities obtained with Method 1 on Uddvide sandstone. Of the three German sandstones presented by Krus (1995), 'Rüthener Sandstein' is most similar to Uddvide sandstone with respect to density, porosity, sorption coefficient for an air dried specimen, and moisture content at capillary saturation (see Table 5.1). The moisture diffusivities obtained with NMR are shown in Figure 5.10.

Table 5.1 Density, porosity and sorption coefficient for an air dried specimen and water content at capillary saturation of four different sandstones.

Sandstone	Density [kg/m^3]	Porosity [%]	*A*-value (air dried specimen) [kg/(m^2·s^{½})]	Moisture content at capillary saturation [kg/m^3]
Baumberger[1]	1980	23	0.044	210
Rüthener[1]	1950	24	0.30	200
Sander[1]	2120	17	0.02	130
Uddvide	2060	23	0.28	160

[1] Krus (1995)

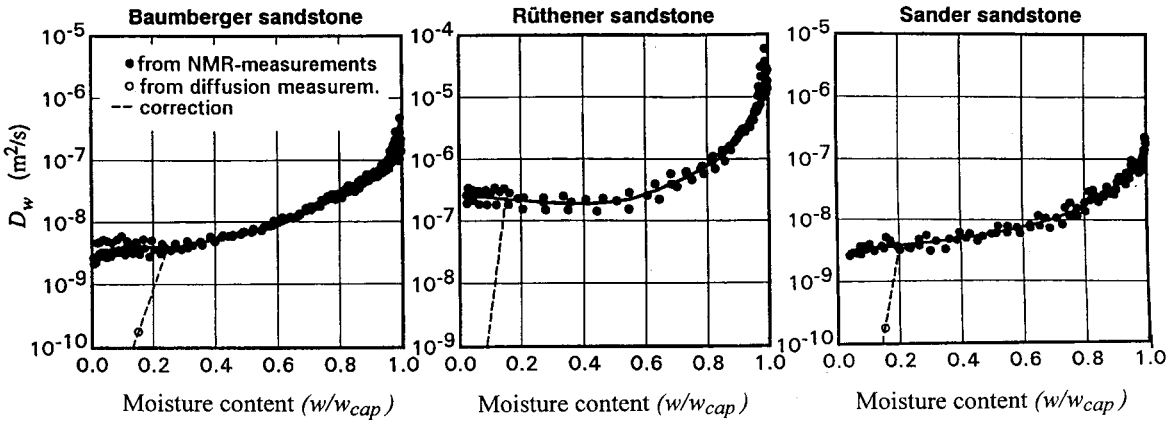

Figure 5.10 Moisture diffusivities obtained with NMR measurements for three German sandstones (Krus 1995).

The same type of calculations that are made on Uddvide sandstone are also made on the autoclaved aerated concrete and bricks reported in Figure 5.5. That is, the moisture diffusivity, $D(w)$ and the Kirchhoff flow potential $\psi(w)$ are calculated with Method 1. The input used is the relation between the initial water content and the sorption coefficient reported by Schwarz (1972) and Gösele et al. (1971) (see Figure 5.5). As shown in the figure, no measurements are reported at the highest initial moisture contents (i.e. when $w_{in} > 265$ kg/m^3 for the autoclaved aerated concrete and $w_{in} > 200$ kg/m^3 for the bricks). The moisture content at capillary saturation is although known for both the autoclaved aerated concrete and the bricks. It is 340 kg/m^3 and 260 kg/m^3 respectively. With these moisture contents at capillary saturation and with the input shown in Figure 5.11 and Figure 5.12, the moisture diffusivities are calculated. The results of the calculation are shown in Figure 5.13.

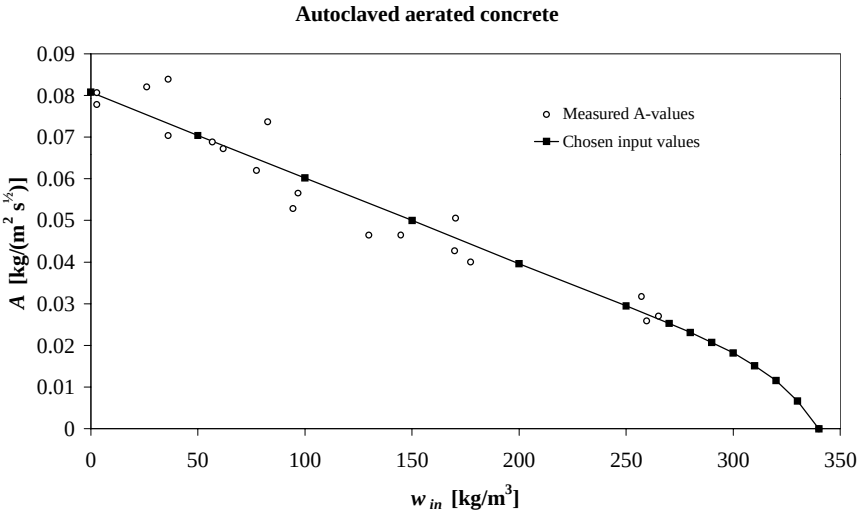

Figure 5.11 The input used for calculating the moisture diffusivity of autoclaved aerated concrete. Measurements reported by Schwarz (1972) and Gösele et al. (1971).

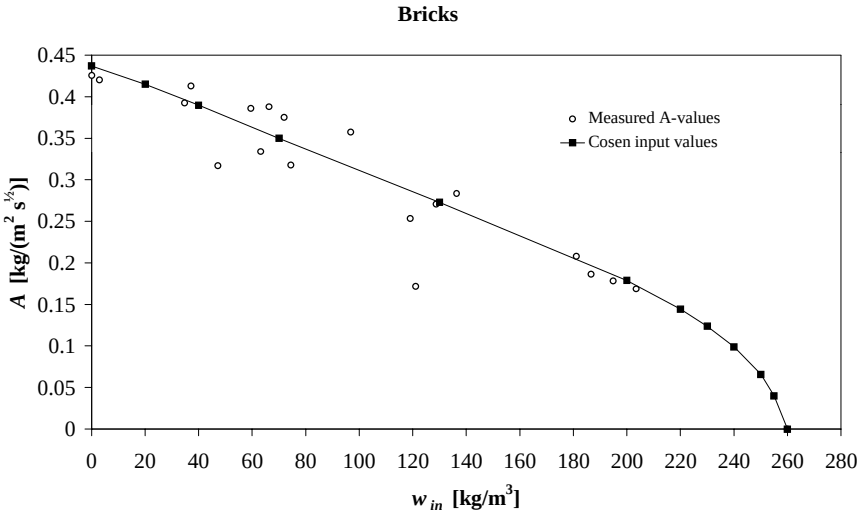

Figure 5.12 The input used for calculating the moisture diffusivity of bricks. Measurements reported by Schwarz (1972) and Gösele et al. (1971).

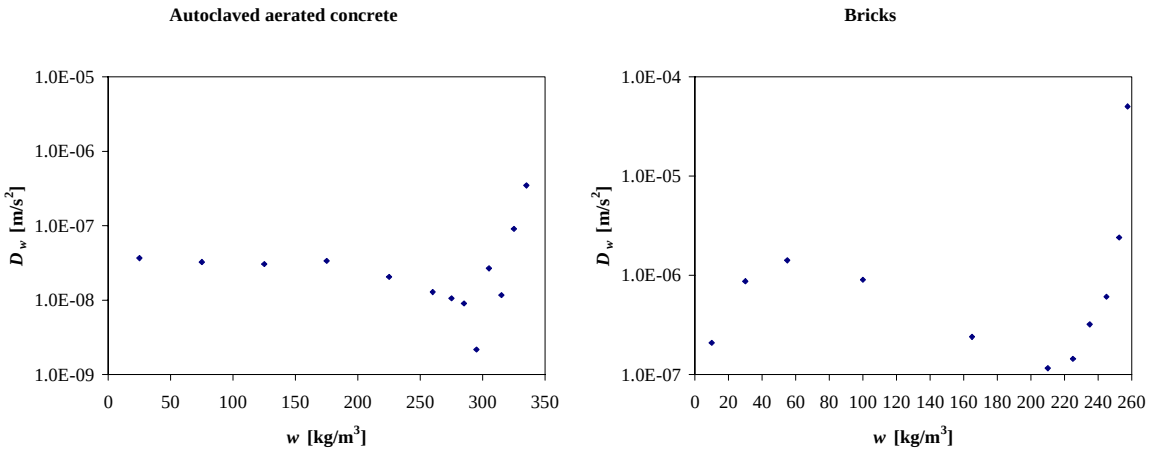

Figure 5.13 Results of calculations of the moisture diffusivity, D(w), performed on autoclaved aerated concrete and bricks. The input used are shown in Figure 5.11 and Figure 5.12.

Moisture diffusivities measured with NMR on types of autoclaved aerated concrete and bricks other than those used by Schwarz (1972) and Gösele et al. (1971) are reported in Krus (1995), (see Figure 5.14). The moisture diffusivities measured with NMR are on the same order of magnitude as those calculated with Method 1, for the materials tested by Schwarz (1972) and Gösele et al. (1971). The moisture diffusivities measured with NMR have more peaks, however, and the moisture diffusivity of bricks changes with time. The moisture diffusivities calculated with Method 1 on the materials tested by Schwarz (1972) and Gösele et al. (1971) have some indication of peaks, however.

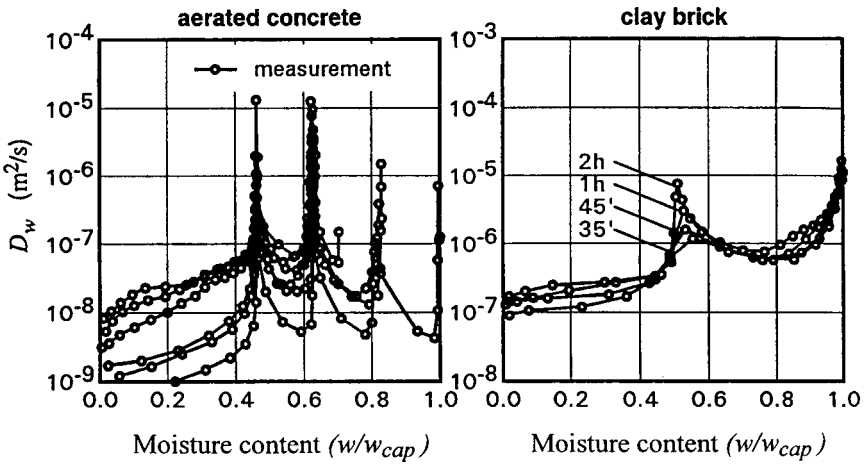

Figure 5.14 Moisture diffusivities measured with NMR on autoclaved aerated concrete and bricks (Krus 1995).

The Kirchhoff flow potential $\psi(w)$ of autoclaved aerated concrete and bricks tested by Schwarz (1972) and Gösele et al. (1971) are calculated in the same way as for Uddvide sandstone above. No known relation $\psi(w)$, determined by the cup-method or any similar method, is used. Therefore ψ is fixed to zero at the lowest moisture content:

$$\psi_{ref} = \psi(w_{min}) = 0 \tag{5.38}$$

Eq. 5.37b - Eq. 5.37c are used to calculate the ψ-values. Eq. 5.37a is not used as there is no known relation for $\psi(w)$. The results of the calculation are given in Figure 5.15.

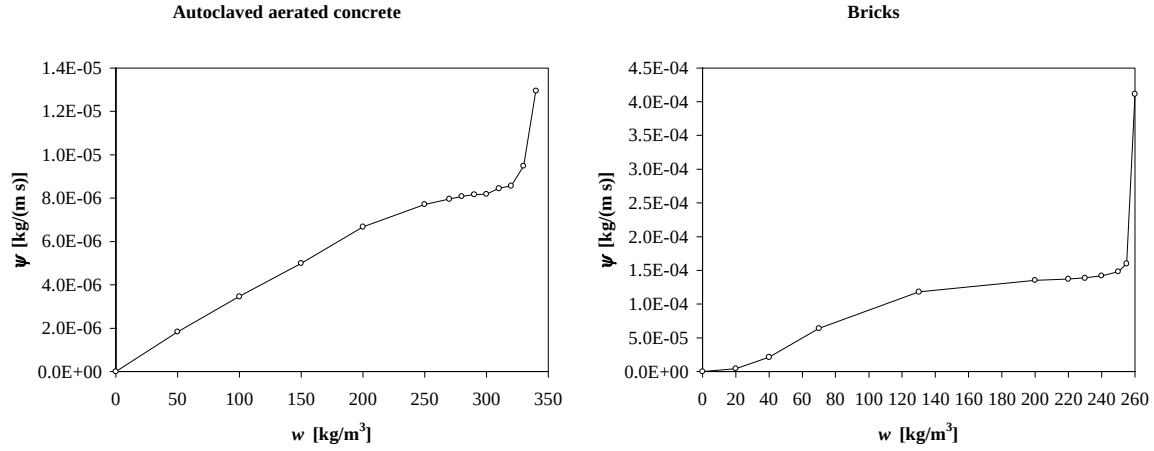

Figure 5.15 The relation $\psi(w)$ of autoclaved aerated concrete and bricks calculated with Method 1on material tested by Schwarz (1972) and Gösele et al. (1971)

5.3.3 Evaluation of the moisture diffusivity with Method 2

It appears from the method of calculation described in section 5.2.4, that the first difference ψ_{cap} - ψ_1 is calculated exactly. The second difference, ψ_{cap} - ψ_2, is calculated with the approximation of A_2' introduced in Eq. 5.27. According to Arfvidsson (1994), the error caused by this approximation is less than 5% if w_1' and ψ_1' are within the limits implied by Eq. 5.27 ($w_1' < 0.5$ and $\psi_1' > 0.5$). When the third difference to the *N*:th difference, ψ_{cap} - ψ_i with $i = 3,..., N$, is calculated an additional approximation is introduced, viz $\psi(w)$ is approximated to be linear for $w_{cap} > w > w_{i-1}$ (see Eq. 5.32 and Figure 5.16). The calculated ψ-values become more uncertain for every calculation step made, as the divergence from the real relation $\psi(w)$ increases (see Figure 5.16). The method gives good results at high moisture contents, near capillary saturation. However, the reliability of the calculated ψ-values decreases with decreasing moisture content.

A calculation with Method 2 is carried out on the Uddvide sandstone with input in accordance with 'Input 3' and 'Input 4' in Figure 5.6 and Appendix A. The incentive for choosing 'Input 3' and 'Input 4' is that Method 2 is more suited for relatively few inputs. As shown by the method of calculation described in section 5.2.4, the calculation results in a relation $\psi(w)$. These results are presented in Figure 5.17.

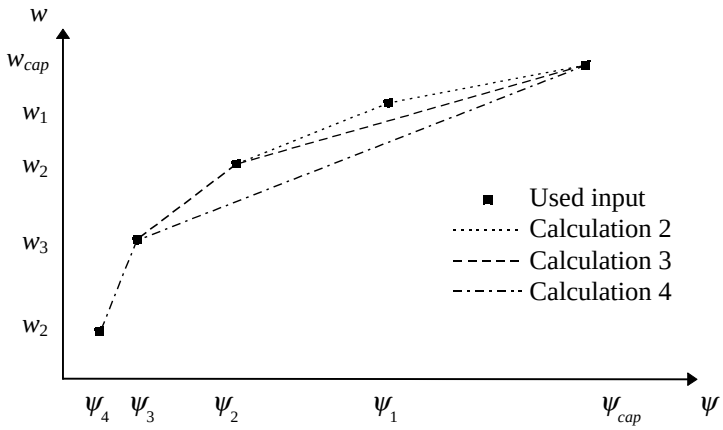

Figure 5.16 ψ_{cap} - ψ_i with i = 3,..., N, are calculated with the Eq. 5.32. $\psi(w)$ is approximated to be linear for $w_{cap} > w > w_{i-1}$. The method gives good results at high moisture contents, near capillary saturation, but the reliability of the calculated ψ-values decrease with decreasing moisture content, while the divergence from the real relation $\psi(w)$ increase.

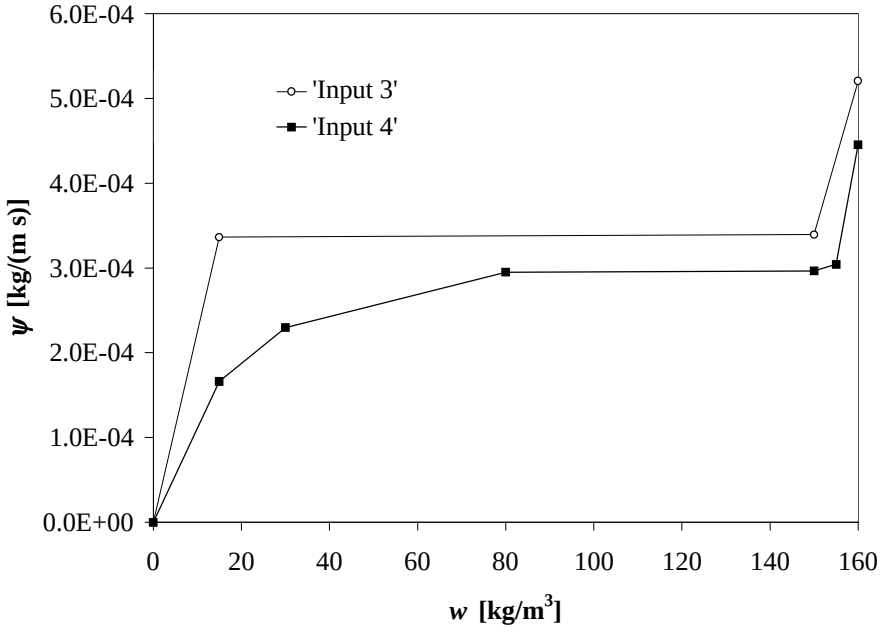

Figure 5.17 Results from calculation of the Kirchhoffs flow potential, ψ(w), made on Uddvide sandstone with Method 2. The calculations are performed on 'Input 3' and 'Input 4', see Figure 5.6 and Appendix A.

In order to make a comparison between Method 1 and Method 2, the moisture diffusivity D_w is calculated from the relation between the Kirchhoff's flow potential and the moisture content $\psi(w)$ by Eq. 5.4:

$$D_w = \frac{\partial \psi}{\partial w}$$

The results of this calculation are shown in Figure 5.18. While the reliability of the calculated moisture diffusivities increases with increasing moisture content, probably only the results obtained at high moisture contents, near capillary saturation, are of practical interest.

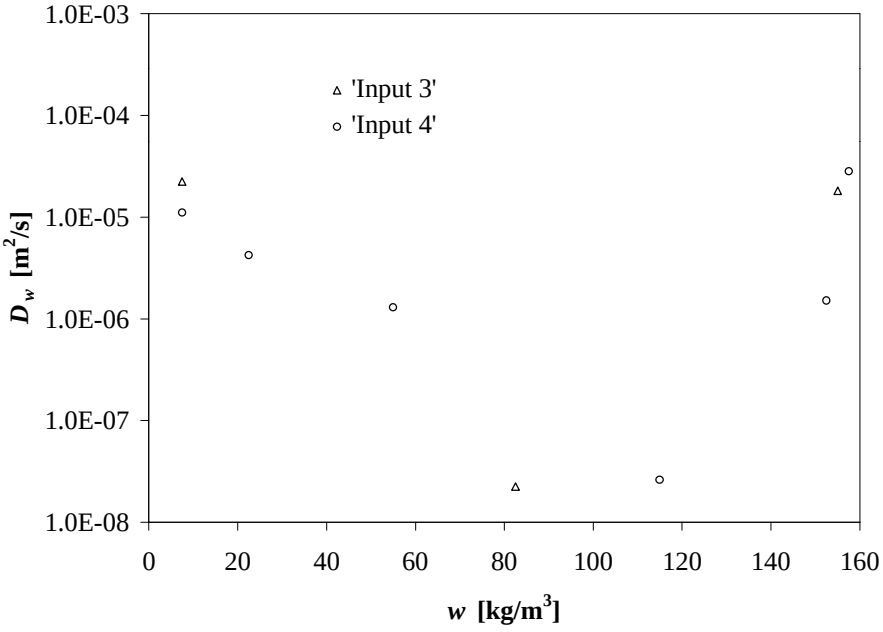

Figure 5.18 Results of calculations of the moisture diffusivity, D(w), on Uddvide sandstone by Method 2. The calculations are performed on 'Input 3' and 'Input 4', see Figure 5.6 and Appendix A.

5.3.4 Comparison between Method 1 and Method 2

The relation among the moisture diffusivity and the Kirchhoff flow potential and the moisture content, $D(w)$ and $\psi(w)$, calculated by Method 1 is exact, if the used mathematical formulation (Eq. 5.1) of capillary transport is correct. Except for the first calculated value, $\psi(w_{max})$, the relations calculated with Method 2 are approximate. The first determined value is calculated in the same way by both methods (compare Eq. 5.14 with Eq. 5.31 and see Figure 5.19 and Figure 5.20):

$$\psi_{Method\,2}(w_{max}) = \psi_{Method\,1}(w_{max}) \tag{5.39}$$

The advantage of Method 2 is that the calculations are easy and quick to perform. The mathematics used in Method 2 is "clean" and it is easy to find solutions for the input chosen. It is considerably more difficult to find solutions by Method 1. As shown in section 5.3.2, the number of possible input values are limited by the inverse of the functions erf(x) and $e_1(x)$ (see Eq. 5.35 and Eq. 5.36). Method 1 is consequently much more time demanding.

Results from calculations made on Uddvide sandstone (using both methods) are shown in Figure 5.19 and Figure 5.20. The input used is 'Input 3' and 'Input 4' (see Figure 5.6). Contrary to the calculations shown in section 5.3.2, the results obtained with the cup-method have not been used in Method 1. Consequently, values calculated with Method 1 for $w < 20$ kg/m^3 are reported in Figure 5.19 and Figure 5.20. The results obtained with the cup method are shown in Figure 5.19. Neither of the methods is applicable to the Uddvide sandstone, for low moisture contents. Both methods must be supplemented at low moisture levels by measurements performed by the cup-method or any other test method. The large error produced by both Method 1 and Method 2 at the low moisture levels do not, however,

influence the calculated values at high moisture levels. This is due to the fact that the calculation starts at capillary saturation for both Method 1 and Method 2.

Furthermore it can be pointed out that both methods give rather similar results, especially at high moisture levels. Besides, the chosen input has no significant effect on the result.

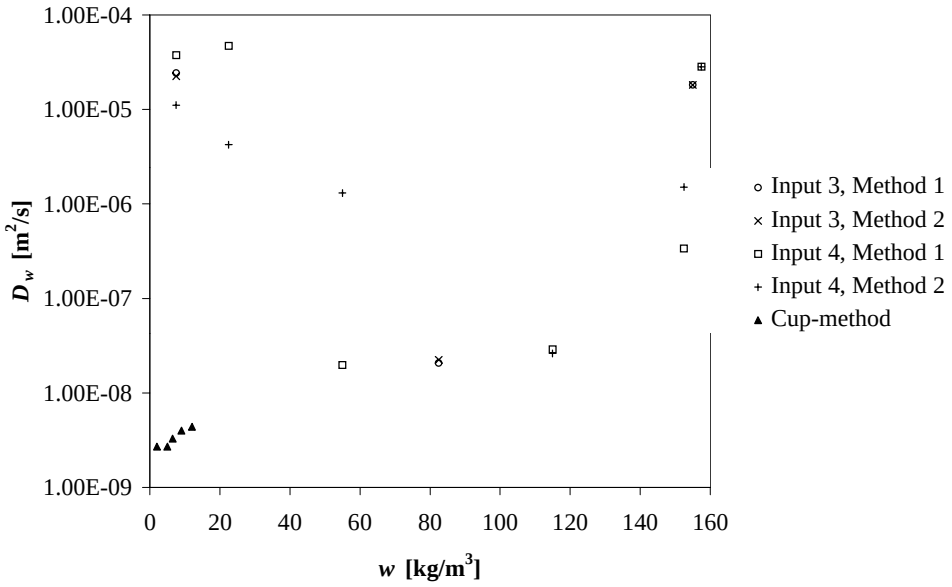

Figure 5.19 The moisture diffusivity of Uddvide sandstone calculated by Method 1 and Method 2. The input used is 'Input 3' and 'Input 4', see Figure 5.6 and Appendix A. Results obtained with the cup-method are also shown (Hedenblad 1996).

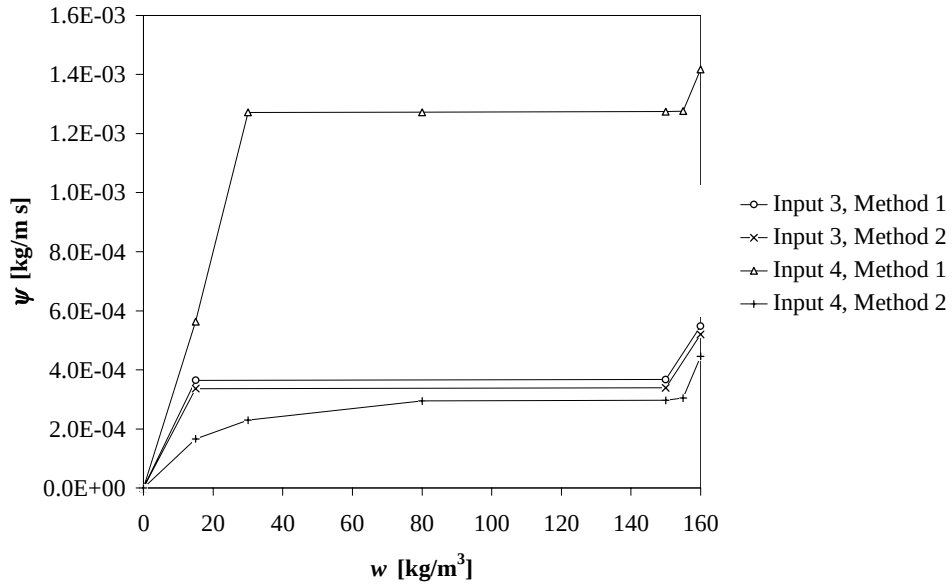

Figure 5.20 The Kirchhoff flow potential of Uddvide sandstone calculated with Method 1 and Method 2. The input used is 'Input 3' and 'Input 4', see Figure 5.6 and Appendix A.

6 References

Adamson, B., Ahlgren, L., Bergström, S. G. and Nevander, L. E. (1970), 'Moisture – Moisture related problems in buildings' (in Swedish), Programskrift 12, Statens råd för byggnadsforskning, Stockholm.

Adan, O.C.G. (1995), 'Determination of moisture diffusivities in gypsum renders', Heron, Vol. 40, No. 3, pp. 201-215.

Ahlgren, L. (1972), 'Moisture fixation in porous building materials', Report 36, Division of Building Materials, Lund Institute of Technology.

Arfvidsson, J. (1994), 'Isothermal moisture transport in porous materials – Calculation and evaluation of material data' (in Swedish), Report TVBH-1007, Division of Building Physics, Lund Institute of Technology.

Arfvidsson, J. and Janz, M. (1994), 'Determination of moisture transport coefficients at very high moisture levels by a series of capillary absorption tests' (in Swedish), Part of Report TVBH-7180, Division of Building Physics, Lund Institute of Technology.

Atkins, P. W. (1994), 'Physical Chemistry' Fifth edition, Oxford University Press.

Bjerkeli, L. (1990), 'X-ray tomography as a method to determine the water adsorption in concrete' (in Norwegian), Report STF65 A90008, FCB, SINTEF, Trondheim.

Brocken, H.J.P. and Pel, L. (1995), 'Moisture transport over the brick/mortar interface', Proceeding of the International symposium on Moisture problems in building walls, Porto, 11-13 Sept., pp. 415-424.

Claesson, J. (1993), 'A few remarks on moisture flow potentials', Report TVBH-7163, Division of Building Physics, Lund Institute of Technology.

Claesson, J. (1994), 'Determination of moisture transport coefficients at very high moisture levels by a series of capillary absorption tests' (in Swedish), Division of Building Physics, Lund Institute of Technology.

Crank, J. (1975), 'The Mathematics of Diffusion', Oxford University Press.

Daian, J-F. (1989), 'Condensation and Isothermal Water Transfer in Cement Mortar: Part II – Transient Condensation of Water Vapour', Transport in Porous Media, Vol. 4, pp. 1-16.

Dawei, M., Chaozong, Z., Zhiping, G., Yisi, L., Fulin, A. and Quitian, M. (1986), 'The application of neutron radiography to the measurement of the water permeability of concrete', Proceedings of the Second World Conference on Neutron radiography, Paris, 16-20 June, pp. 255-262.

Descamps, F. (1990), 'Moisture content measurement using gamma ray attenuation' Research Report, Laboratorium Bouwfysica, Katholieke Universitet Leuven.

Fagerlund, G. (1977), 'The critical degree of saturation method of assessing the freeze/thaw resistance of concrete', Materials and Structures, Vol. 10, No. 58.

Fagerlund, G. (1993), 'The long time water absorption in the air-pore structure of concrete', Report TVBM-3051, Division of Building Materials, Lund Institute of Technology.

Freitas, V. P. De, Krus, M., Künzel, H. and Quenard, D. (1995), 'Determination of the water diffusivity of porous materials by gamma-ray attenuation and NMR', Proceeding of the International symposium on Moisture Problems in Building Walls, Porto, 11-13 Sept, pp. 445-460.

Gösele, K., Künzel, H. and Schwarz, B. (1971), 'Capillary water transport in building materials' (in German), Az.: I6-800169-18, Institut für technische Physik, Stuttgart/Holzkirchen.

Hall, C. (1994), 'Barrier performance of concrete: A review of fluid transport theory', Materials and Structures, Vol. 27, pp. 291-306.

Hedenblad, G. (1993), 'Moisture Permeability of Mature Concrete, Cement Mortar and Cement paste', Report TVBM-1014, Division of Building Materials, Lund Institute of Technology.

Hedenblad, G. (1996), 'Material properties for calculations of moisture transport' (in Swedish), Report T19:1996, Swedish Council for Building Research, Stockholm.

Holmes, A. (1965), 'Principles of Physical Geology', Thomas Nelson and sons Ltd, London.

Hägg, G. (1984), 'General- and inorganic chemistry' (in Swedish), Almqvist & Wiksell, Uppsala.

International Standard (ISO 9346: 1987 E), 'Thermal insulation - Mass transfer - Physical quantities and definitions', First edition, Reference number: ISO 9346: 1987 (E).

Janz, M. (1995), 'Capillary water uptake test on a calcareous sandstone - Methods and results' (in Swedish), Report TVBM-7097, Division of Building Materials, Lund Institute of Technology.

Johannesson, B. (1996), Personal communications, Division of Building Materials, Lund Institute of Technology.

Jonasson, S. A. (1991), 'Estimation of soil water retention for natural sediments from grain size distribution and bulk density', Publ. A 62, Department of Geology, Chalmers University of Technology and University of Göteborg.

Justnes, H., Bryhn-Ingebrigtsen, K. and Rosvold, G. O. (1994), 'Neutron radiography: an excellent method of measuring water penetration and moisture distribution in cementitious materials', Advances in Cement Research, Vol. 6, No. 22, pp. 67-72.

Kießel, K. and Krus, M. (1991), 'NMR-measurements of capillary penetration behaviour of water and hydrophobing agent in porous stone and derivation of new capillary transport values', Report FtB-12e, Fraunhofer-Institut für Bauphysik, Holzkirchen.

Kießel, K., Krus, M. and Künzel, H. (1993), 'Advanced measuring and calculative procedures for moisture assessment of building elements. Examples of practical applications, (in German), Bauphysik 15, Heft. 2.

Kopinga, K. and Pel, L. (1994), 'One-dimensional scanning of moisture in porous materials with NMR', Rev. Sci. Instrum. 65 (12).

Krus, M. and Kießl, K. (1991), 'An experimental comparison between pore size distributions obtained with mercury porosimetry and pressure extractors' (in German), Report FtB-11, Fraunhofer-Institut für Bauphysik, Holzkirchen.

Krus, M. (1995), 'Moisture transport and storage coefficients of porous mineral building materials. Theoretical principles and new test methods' (in German), der Fakultät Bauingenieur- und Vermessungswesen der Universität Stuttgart.

Künzel, H. M. (1995), 'Simultaneous Heat and Moisture Transport in Building Components – One- and two-dimensional calculation using simple parameters', IRB Verlag, Stuttgart.

Lindborg, U. (1990), 'Air pollution and the cultural heritage - Action plan 90', Report RIK 1, The Central Board of National Antiquities and the National Historical Museum, Stockholm.

Letey, J., Osborn, J. and Pelishek, R. E. (1962), 'Measurement of liquid-solid contact angles in soil and sand', Soil Science, Vol. 93, No. 3, pp. 149-153.

Nielsen, A. F. (1972), 'Gamma-Ray-Attenuation used for Measuring the Moisture Content and Homogeneity of Porous Concrete', Building Science, Vol. 7, pp.257-263.

Nielsen, D. R., van Genuchten, M. Th. and Biggar, J. W. (1986), 'Water Flow and Solute Transport Process in the Unsaturated Zone', Water Resources Research, Vol. 22, No. 9, pp. 89S-108S.

Nilsson, L.-O. (1980), 'Hygroscopic moisture in concrete - Drying measurements and related material properties, Report TVBM-1003, Division of Building Materials, Lund Institute of Technology.

Pel, L. (1995), 'Moisture transport in porous building materials', Eindhoven University of Technology.

Quernard, D. and Sallee, H. (1989), 'A gamma-ray spectrometer for measurement of the water diffusivity of cementitious materials', Materials Research Symposium Proceedings, Boston, 28-30 November, Vol. 137, pp. 165-169.

Sandin, K. (1978) 'A method of measuring the moisture distribution in aerated autoclaved concrete' (in Swedish), Division of Building Materials, Lund Institute of Technology.

Schwarz, B. (1972), 'Capillary water absorption in building materials' (in German), Gesundheits-Ingenieur, Heft 7, Nr. 93.

Sosoro, M. (1995), 'A model to predict the absorption of organic fluids in concrete' (in German), Deutscher Ausschuß für Stahlbeton, Heft 446, Beuth Verlag GmbH, Berlin.

Sosoro, M. and Reinhardt, H. W. (1995), 'Thermal imaging of hazardous organic fluids in concrete', Materials and Structures, Vol. 28, No. 183, pp. 526-533.

van Brakel, J. (1975), 'Pore Space Models for Transport Phenomena in Porous Media - Review and Evaluation with Special Emphasis on Capillary Liquid Transport', Powder Technology, 11, pp. 205-236.

Volkwein, A. (1991), 'Investigation of absorption of water and chloride in concrete' (in German), Heft 1/1991, Institute of Building Materials, Technical University of Munich.

Volkwein, A. (1993), 'The capillary suction of water into concrete and the abnormal viscosity of the porewater', Cement and Concrete Research, Vol. 23, pp. 843-852.

Vos, B. H. (1965), 'Non-steady-state Method for the Determination of Moisture Content in Structures', Humidity and Moisture, Vol. 4, pp. 35-47, New York.

Weast, R. C., Lide, D. R., Astle, M. J. and Beyer, W. H. (1989), 'Handbook of Chemistry and Physics', 70TH edition, CRC Press, Inc. Boca Raton, Florida.

Wessman, L. and Carlsson, T. (1995), 'Characterisation of some Swedish natural stones with thin section microscopy' (in Swedish), Report TVBM-7095, Division of Building Materials, Lund Institute of Technology.

Wessman, L. (1996), 'Deterioration of natural stone by freezing and thawing in salts solutions', Proceedings, Durability of Building Materials and Components 7, Stockholm, 19-23 May, Vol. 1, pp. 342-351.

Wittig, G. and Lingott, H. (1992), 'Investigation of the moisture transport in building materials by microwave beam' (in German), Bauphysik 14, Heft 2, pp. 44-49.

Wormald, R. and Britch, A.L. (1969), 'Methods of Measuring moisture Content Applicable to Building Materials', Building Science, Vol. 3, pp.135-145.

Appendix A

Input data

The input data, i.e. the initial moisture contents w_{in} and the sorption coefficients A, used for the calculations of the moisture diffusivity of Uddvide sandstone. The moisture content at capillary w_{cap} saturation always is 160 kg/m^3.

Input 1		Input 2		Input 3		Input 4	
w_{in} [kg/m^3]	A [kg/(m^2·s)]	w_{in} [kg/m^3]	A [kg/(m^2·s)]	w_{in} [kg/m^3]	A [kg/(m^2·s)]	w_{in} [kg/m^3]	A [kg/(m^2·s)]
159	0.012	159	0.014	150	0.048	155	0.03
158	0.0194[1]	158	0.0227[1]	15	0.227[1]	150	0.0485[1]
157	0.0247[1]	157	0.0289[1]	0	0.28	80	0.15[1]
156	0.0291[1]	156	0.034[1]			30	0.193[1]
155	0.0329[1]	155	0.0385[1]			15	0.22
154	0.0364[1]	154	0.0425[1]			0	0.279
153	0.0395[1]	153	0.0462[1]				
152	0.0425[1]	152	0.0496[1]				
151	0.0453[1]	151	0.0529[1]				
150	0.0479[1]	150	0.0559[1]				
145	0.0591[1]	145	0.0691[1]				
140	0.0685[1]	140	0.0802[1]				
80	0.145	80	0.1619[1]				
70	0.1553						
60	0.1648						
50	0.1733[1]						
40	0.1815[1]						
30	0.1891[1]						
20	0.2065						
10	0.2341						
0	0.28						

[1] The lowest possible *A*-value are used.